

Robust semi-parametric signal detection in particle physics with classifiers decorrelated via optimal transport ^{*}

Purvasha Chakravarti [†]

Department of Statistical Science, University College London

Lucas Kania [†]

Department of Statistics & Data Science, Carnegie Mellon University

Olaf Behnke

Deutsches Elektronen-Synchrotron (DESY)

Mikael Kuusela and Larry Wasserman

Department of Statistics & Data Science, Carnegie Mellon University

Abstract

Searches for new signals in particle physics are usually done by training a supervised classifier to separate a signal model from the known Standard Model physics (also called the background model). However, even when the signal model is correct, systematic errors in the background model can influence supervised classifiers and might adversely affect the signal detection procedure. To tackle this problem, one approach is to use the (possibly misspecified) classifier only to perform a preliminary signal-enrichment step and then to carry out a bump hunt on the signal-rich sample. For this procedure to work, we need a classifier constrained to be decorrelated with one or more protected variables used for the signal-detection step. We do this by considering an optimal transport map of the classifier output that makes it independent of the protected variable(s) for the background. We then fit a semi-parametric mixture model to the distribution of the protected variable after making cuts on the transformed classifier to detect the presence of a signal. We compare and contrast this decorrelation method with previous approaches, show that the decorrelation procedure is robust to moderate background misspecification, and analyze the power and validity of the signal detection test as a function of the cut on the classifier both with and without decorrelation. We conclude that decorrelation and signal enrichment help produce a stable, robust, valid, and more powerful test.

Keywords: Large Hadron Collider, bump hunt, model misspecification, high-energy physics, mixture density fitting, semi-parametric hypothesis testing.

^{*}The authors gratefully acknowledge NSF grants PHY-2020295, DMS-2053804 and DMS-2310632.

[†]These two authors contributed equally to this paper. The names are in alphabetical order.

1 Introduction

Particle physics aims to understand the structure of matter at a fundamental level, i.e., to discern those particles that compose matter but cannot be decomposed. The Standard Model (SM) of particle physics provides the theory behind all known fundamental particles and their interactions. For a long time, physicists have theorized about the existence of multiple new fundamental particles beyond the SM and are now searching for empirical evidence of these particles [Evans and Bryant, 2008].

Many experiments are conducted at particle colliders, where particles are accelerated to almost the speed of light and then made to collide, to search for these theorized particles. In the Large Hadron Collider (LHC), two protons or heavy ions are accelerated in opposite directions and made to collide within four underground detectors – ALICE, ATLAS, CMS, and LHCb. When a collision occurs, the kinetic energy of the particles transforms into mass, creating new particles [Lyons, 2008]. The new particles formed are often unstable, called resonances, which almost instantly decay into other more stable particles. The paths of these particles, along with their momenta and energies, are recorded within the particle detectors. By measuring these, scientists can reconstruct the properties of the unstable particles that gave rise to these more stable, observable particles. Each collision is referred to as an event. Most collisions are considered uninteresting and constitute what physicists call background events. However, some collisions might create the theorized fundamental particles. Hence, the problem is to separate those collisions of interest, called the signal events, from the background events. Two examples of signal events that we discuss in the experiments of this paper are high-momentum W-boson production (described below) and high-mass resonance production (described in further detail in Appendix A.1).

Some theorized new massive particles are predicted to decay into a final state containing

a W-boson and other heavy particles [ATLAS, 2018b]. However, the W-boson itself is an unstable resonance and can decay into two quarks, which produce collimated streams of particles, called jets. The presence of the heavy particles causes the W-boson to have an unusually high transverse momentum (p_T) and the two jets from the W-boson decay to merge into a single large-radius “W-jet”. This is an example of new physics searches where the task is to discriminate the hadronically decaying W-bosons (signal events) from the large group of events that produce non-resonant jets (background events). For W-bosons, the invariant mass of the resulting large-radius jet is a good discriminator from the non-resonant background since the signal is localized in mass forming a peak, whereas the background is smooth [ATLAS, 2018b]. While the W-boson itself is a well known SM particle, detecting highly boosted W-bosons via their mass peak signal can be a strong indirect hint for new resonances with much higher mass.

Now, it is well-established that W-jets have a rich jet substructure characterized by the patterns and distributions of the particles within the jet. Training boosted decision trees and neural network classifiers on jet substructure variables (see Table 1 in ATLAS [2018b]) has proven to be particularly successful in increasing the power of detecting the signal events [ATLAS, 2017a,b]. However, these classifiers are trained on Monte Carlo simulations from the hypothesized models, with access to the simulated true labels, but evaluated on unlabelled experimental collision data. Since simulating jets accurately is difficult, there might be systematic differences between the training and the test data. Additionally, the data generation process might not be uniquely specified, with the presence of nuisance parameters, which would also cause differences between the training and test data, affecting the trained classifiers [Louppe et al., 2017].

The solution is to use a variable in which the signal detection test can be performed

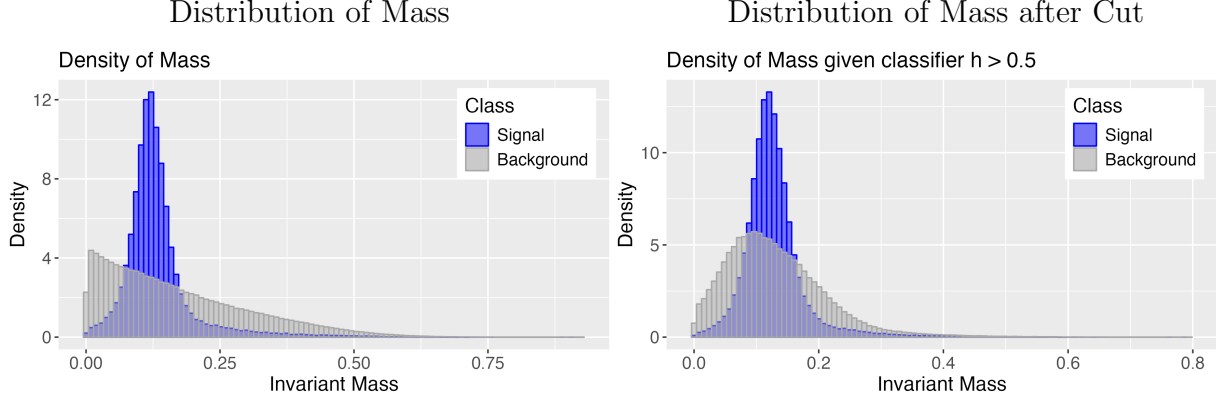


Figure 1: Evidence of sculpting in the shape of the background distribution.

without having access to reliable background samples. A common choice is a variable (e.g. invariant mass above) in which the signal is localized and the background is smooth, so that the signal detection test can be performed as a bump hunt [CDF Collaboration, 2009, Choudalakis, 2011]. However, we also have supervised classifiers trained on auxiliary variables (e.g., jet substructure variables for W-boson and kinematic variables for the high-mass resonance event). We can use these to perform a filtering step to enhance the signal before using the invariant mass for the actual test. The classifiers however exhibit a non-linear dependence with the invariant mass and a filtration based on them distorts the shape of the invariant mass distribution for the background events, making it hard to distinguish it from the signal events. This phenomenon is called *sculpting* (see Figure 1). Hence, the objective is to find a classifier that is independent (called decorrelation in high-energy physics) with invariant mass [ATLAS, 2018b]. More generally, we want a classifier that is decorrelated with respect to *protected variable(s)* in which the bump hunt will be performed.

This paper presents a data analysis pipeline consisting of a decorrelation algorithm and a signal detection test and show the robustness of the framework to systematic mismodeling of the background data. Our experiments also show that using the decorrelated classifiers to incorporate auxiliary information does indeed increase the power of the signal

detection test, while filtering using non-decorrelated classifiers yields unreliable tests due to sculpting.

1.1 Introduction to bump hunting

The detection of new physical phenomena in high-energy physics has historically relied on the search for resonances causing a bump in the invariant-mass spectrum of their daughter particles. The shape of the bump is driven by the natural width of the resonance as well as by detector resolution effects. Physical background processes are known to usually produce smooth mass distributions. Thus, the presence of deviations from this pattern can provide evidence for the existence of undiscovered phenomena. Although physicists might not know the exact background or signal distributions, they can often pinpoint regions of the invariant mass spectrum where they expect to observe a resonance if it exists. These are called signal regions. These two assumptions, smoothly decaying background and known signal regions, can be used to perform signal detection. To make the ideas concrete, consider figure 2a, which presents an idealized scenario in which we have data from a mixture of background and signal events and a predefined signal region. First, the background is estimated while censoring the signal region; see Figure 2b. Second, the fitted background is interpolated to the signal region; see Figure 2c. Finally, the physicists check if the observed distribution differs significantly from the interpolated fitted background; see Figure 2d.

This methodology is called *bump hunting* [CDF Collaboration, 2009] and goes back at least to the discovery of the ρ meson [Button et al., 1962]. A successful improvement has been the `BumpHunter` algorithm [Choudalakis, 2011] that searches the entire invariant mass spectrum using a moving signal region while accounting for performing multiple hypothesis tests, called the *look elsewhere effect* in the physics literature [Gross and Vitells, 2010]. The

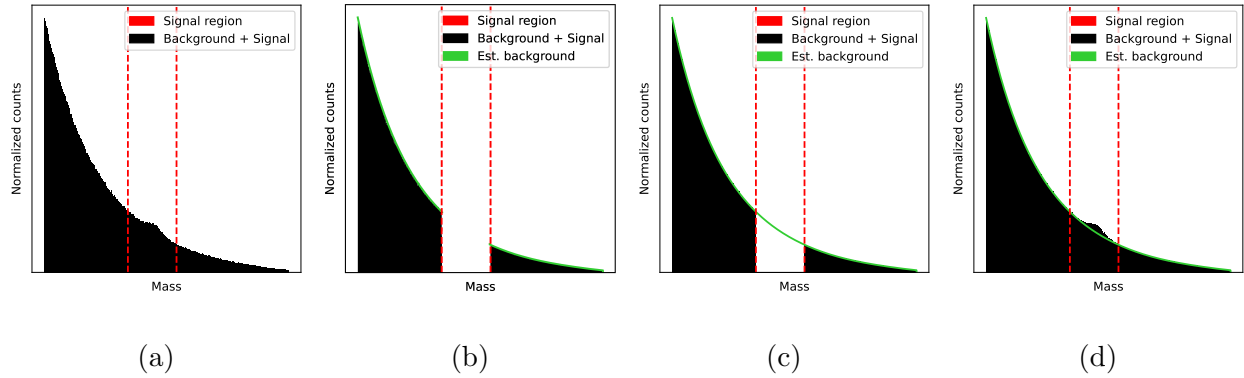


Figure 2: Pictorial representation of bump hunting.

algorithm has been widely used together with parametric and non-parametric background estimation [ATLAS Collaboration, 2010, CDF Collaboration, 2009]. Modern developments have focused on using machine learning both to estimate the background and to improve the sensitivity of signal tests through classifiers [Kasieczka, 2021]. For instance, Collins et al. [2019] uses classifiers to enrich the signal region and then proceeds to perform a likelihood ratio test with a parametric background and model-free signal using the asymptotic formulae proposed by Cowan et al. [2011]. Although asymptotically valid, such an approach is not necessarily optimal. In this work, we prove the asymptotic optimality of the proposed test in section 2.2 via the semi-parametric framework. That is, the test asymptotically makes the most efficient use of the available data while allowing for an arbitrarily complex signal contained in the signal region.

1.2 Introduction to decorrelation

Bump hunting requires a reasonably large signal strength to detect the presence of signal events. However, in many new physics searches, the expected signal strengths are small, leading to negligible power when testing. Hence, a supervised classifier (h) trained on available auxiliary variables of the simulated background and signal samples is used to identify signal-rich regions where the background is suppressed. The bump hunt search is

then performed on the data within this signal-rich region given by predetermined *cuts* on the classifier output [ATLAS, 2018b]. If the classifier (h) is trained so that large values correspond to signal events, for a cut at $t \in [0, 1]$, the signal-rich region is given by $\{x : h(x) > t\}$. (Note: this is different from the signal region in Figure 2a.) The bump hunt now is performed conditioned on the classifier, which changes (sculpts) the smooth background distribution of the protected variable, making it hard to distinguish it from the signal distribution (see Figure 1). This would make the bump-hunt test lose validity since, under the null case, the data has a bump.

To ensure that the background distribution remains unchanged after signal enrichment, it is sufficient to use a classifier that is independent of the protected variable. This can be achieved in three ways: (1) Make the input variables of the classifier independent. (2) Enforce the classifier to be independent during training. (3) Transform any pre-trained classifier to be independent by composing the classifier output with an additional mapping. Our algorithm CDOT (Classifier Decorrelated using Optimal Transport) takes this approach using an optimal transport map.

Early works took the first approach by using theoretical domain knowledge to modify the auxiliary variables before training the classifier to achieve independence. Examples include Designing Decorrelated Taggers (DDT) [Dolen et al., 2016] and the Convolved Sub-Structure (CSS) approach [Moult et al., 2018]. These two methods are specific to particular experiments and do not utilize the full potential of all available auxiliary variables.

To perform decorrelation during the training stage, one approach is to add a penalty term to the classification loss function when fitting the classifier. Multiple penalty terms have been considered in past literature, e.g., DisCo [Kasieczka and Shih, 2020] uses the distance correlation. Adversarial Neural Networks (ANN) [Shimmin et al., 2017, Louppe

et al., 2017] use as penalty the accuracy of a second adversary neural network that predicts the protected variable from the classifier output, maximizing classification accuracy while minimizing the dependence of the classifier output on the protected variable. Moment Decomposition (MoDe) [Kitouni et al., 2021], on the other hand, argues that we do not need independence, instead they ensure that the trained penalized classifier does not introduce a localization (bump) in the background by adding a penalty based on the moments of the protected variable’s CDF. Other examples include the outlier exposure variational autoencoders (OE-VAE) [Cheng et al., 2023].

This paper and a parallel body of work CNOTS [Algren et al., 2024] take the last approach. Both works find a transformation of a pre-trained classifier that makes it independent of the protected variable using an optimal transport map [Villani, 2021]. However, the methods diverge in the way they estimate the map. We find a closed-form solution to the optimal transport problem and estimate it using conditional kernel density estimators. CNOTS uses the Kantorovich dual formulation of the problem to show that the optimal transport map can be written as the gradient of a convex neural network. The authors then fit two partially input convex neural networks (PICNNs) to estimate this. Both methods are applicable to multivariate protected variables. CNOTS additionally handles multivariate classifiers, whereas we address univariate classifiers. We note that our method can be extended to multivariate classifiers, but the optimal transport problem does not have a closed-form solution in that case (except for when they are normally distributed) and needs to be estimated numerically, making it computationally expensive.

Klein and Golling [2022] find the transformation using a conditional normalizing flow that finds a map between the conditional distribution of the classifier given the protected variables and a known distribution using a neural network. In Moreno et al. [2020], instead

of transforming the classifier, they change the cut threshold such that the distribution of the protected variable after the cut remains unchanged for the background. They perform quantile regression of the classifier output on the protected variable to estimate the threshold as a function of the protected variable corresponding to a particular quantile t . In theory, this is identical to finding a transformed classifier and fixing the threshold at t , but the way the estimation is performed in practice is different. Additionally, in this case, the threshold is a random variable that varies with the protected variable.

1.3 Contributions

Our main contribution is to present a complete pipeline for signal detection using a decorrelated classifier and provide a statistical analysis of the entire pipeline. We study—to the best of our knowledge, for the first time—how implementing a classifier filtration and a decorrelation algorithm before performing a bump hunt affects the power and validity of the signal detection test compared to not implementing them. The pipeline consists of three steps – (i) *Training Classifier*: Train a classifier to separate the signal from the background using auxiliary variables; (ii) *Signal Enrichment*: (a) Apply the proposed decorrelation algorithm based on optimal transport to the trained classifier; (b) Filter data using the decorrelated classifier; (iii) *Signal Detection*: Use a semi-parametric bump-hunt test on the filtered data to perform signal detection. A flowchart is provided in Appendix A.2.

The decorrelation algorithm we propose can also be extended via geodesic morphing to give rise to a range of classifiers with varying degrees of decorrelation. The intermediate stages provide higher signal vs. background separation than the completely decorrelated classifier and higher decorrelation than the original classifier. We compare our proposed decorrelation method with previous decorrelation methods as a function of the degree of

decorrelation and demonstrate the superiority of the method for high levels of decorrelation.

Regarding bump hunting [CDF Collaboration, 2009, Choudalakis, 2011], for flexible parametric background distributions and arbitrary signal distributions, we propose a test based on the protected variable and prove its optimality in the semi-parametric framework [van der Vaart, 1998]. Informally, the optimality guarantees that the proposed test makes the best use of the available information when the signal is arbitrarily complex but contained in the signal region. The test is based on computing the maximum likelihood estimator while censoring the signal region and is connected to previous work on counting experiments and interpolating the background distribution on the signal region [Behnke et al., 2013]. Since the test is performed after the signal enrichment step, we propose a simple model selection procedure based on sample splitting to empirically calibrate the test under the null distribution.

We perform a robustness study of the signal detection pipeline to systematic misspecification of the background distribution. To the best of our knowledge, this is the first robustness study in decorrelation literature. We study the power and validity of the signal detection test with and without decorrelation and with and without signal enrichment and conclude that decorrelation and signal enrichment help produce a stable, robust, valid, and more powerful test. Lastly, one of our objectives is to also introduce the idea of decorrelation to statisticians since it has potential applications outside of particle physics.

2 Methods

As discussed in the introduction in Section 1, we have three sources of data at hand

$$\text{MC Background } (\mathcal{B}) : \quad X_1, \dots, X_{m_b} \sim p_b$$

$$\text{MC Signal } (\mathcal{S}) : \quad Y_1, \dots, Y_{m_s} \sim p_s$$

$$\text{Experimental/Real data } (\mathcal{E}) : \quad W_1, \dots, W_n \sim q = (1 - \lambda) \cdot p_b + \lambda \cdot p_s$$

Here p_b , p_s , and q are the densities of the simulated background, the simulated signal, and the experimental data, respectively. $\lambda \in [0, 1]$ is the signal strength which represents the probability of a signal event in the experimental data. Furthermore, we have data on the protected variable M , for all the three samples, i.e., $M_i^X \sim p_{bM}$ (Background), $M_i^Y \sim p_{sM}$ (Signal) and $M_i \sim q_M$ (Experimental, for brevity). Henceforth, we will drop the M from the density notation to interchangeably use p_b , p_s , and q for the protected variable as well, since from context, it should be clear which density we mean. We want to perform a signal detection test, i.e., test $H_0 : \lambda = 0$. As discussed in Section 1, since the signal is localized in the protected variable, the test is performed on the protected experimental data $M_i \sim q = (1 - \lambda)p_b + \lambda p_s$. Additionally, as explained in the introduction, we do not entirely trust the background simulations and so, do not use the background or signal simulations for the actual test. Hence, the test is able to robustly detect any signal that is localized in the protected variable, even if the background simulation is misspecified.

Let $S \in \{0, 1\}$ be an indicator for a signal event. Now, let $Z = h(W) = \hat{\mathbb{P}}(S = 1|W)$ denote the output of a probabilistic classifier that separates background and signal data. The joint density of (Z, M) for the experimental data can be written as

$$p(z, m) = p(z)[(1 - \lambda(z))p_b(m|z) + \lambda(z)p_s(m|z)], \quad (1)$$

where $\lambda(z) = \mathbb{P}(S = 1|Z = z)$. Now, $\lambda = \mathbb{P}(S = 1) = \int \lambda(z)dP(z)$. We want to test

$H_0 : \lambda = 0$. But as described in Section 1, we want to perform the test after performing signal enrichment, i.e., perform the test on experimental data that passes the cut: $Z = h(W) > t$, where $t > 0$ is some fixed threshold. So, instead of λ we are now interested in $\lambda(z)$ for $z > t$. Under the null, $H_0 : \lambda = 0$, we also have $\lambda(z) = 0 \forall z$. Also, we expect $\lambda(z)$ to increase as z increases since the classifier is trained to detect signal, so higher classifier output indicates a higher chance of the event being a signal event.

Considering the conditional density $p(z, m | Z > t)$, this has two effects: we are now interested in $\lambda(z)$ for $z > t$ which is larger than λ , so it increases the signal strength in the test data (good) but it replaces $p_b(m)$ and $p_s(m)$ with $p_b(m | Z > t)$ and $p_s(m | Z > t)$ which are closer together (bad) causing sculpting. Ideally, we want the optimal classifier subject to the condition: $p_b(m|z) = p_b(m)$ and $p_s(m|z) = p_s(m)$. It is impossible to satisfy both of these conditions at once but in practice, it is sufficient to have $Z = h(W)$ such that $p_b(m|z) = p_b(m)$, i.e., h is constructed so that $h(X)$ is independent of $m(X)$, given that X is from the background distribution p_b . Note also that as the amount of enrichment (t) increases, while $\lambda(z)$ increases, the sample size decreases, and hence, too much enrichment could potentially reduce power. So there is a trade-off between sample size and increasing $\lambda(z)$ and one needs to be careful when choosing t . So, now the joint density of (Z, M) becomes: $p(z, m) = p(z)[(1 - \lambda(z))p_b(m) + \lambda(z)p_s(m|z)]$ due to decorrelation.

The proposed signal detection workflow has three steps (see flowchart in Appendix A.2):

(Step 1): Training and Decorrelation: Train a probabilistic classifier (h) on the simulated signal and simulated background data to identify signal events. Then apply a transformation ($T_M(h)$) to decorrelate it, i.e., make it independent of the protected variable (M) for the background. We present the decorrelation procedure where we find the transformation T_M using optimal transport in more detail in Section 2.1.

(Step 2): Signal Enrichment: Filter the experimental data (W 's) using the classifier selecting a signal-rich sub-sample $E_t = \{i : T_{M_i}(h(W_i)) > t\}$ for some threshold $0 < t < 1$.

(Step 3): Signal Detection: We perform a bump-hunt on the protected variable for the selected experimental data, i.e., on M_i for $i \in E_t$. Let M be distributed as $q(m) = (1 - \lambda) \cdot p_b(m) + \lambda \cdot p_s(m)$. Here, $p_b(m)$ is a smooth background model, and $p_s(m)$ is a bump-like function. We additionally have for the selected experimental data:

$$q(m|Z > t) = (1 - \lambda_t) \cdot p_b(m) + \lambda_t \cdot p_s(m|Z > t) \quad (2)$$

where $Z = T_M(h(W))$ is the new transformed classifier and $\lambda_t = \mathbb{P}(S = 1|Z > t)$.

We fit $q(m|Z > t)$ using the selected experimental data, M_i for $i \in E_t$, and test $H_0 : \lambda_t = 0$ versus $H_1 : \lambda_t > 0$. We discuss the signal detection in detail in Section 2.2.

2.1 Decorrelation via optimal transport

The goal of the decorrelation procedure is to construct h so that $h(X)$ is independent of $m(X)$, given X is from the background distribution p_b . One option is to transform the data X to make it independent of M for $X \sim p_b$. However, if X is high-dimensional, this is computationally expensive, and a practical alternative is to consider transforming the classifier $h(X)$ to be independent of M for $X \sim p_b$. We want to do this such that the transformed classifier output is as close to the original as possible, while keeping the marginal distribution the same. Without loss of generality, one could choose any distribution for the new marginal distribution. We decided to keep the marginal distribution unchanged.

One way to achieve this transformation is by solving the optimal transport problem given by: minimizing $\mathbb{E}[(T_M(Z) - Z)^2]$ subject to $T_M(Z)$ independent of M and $p_{bT_M(Z)}(z) = p_b(z)$, where $Z = h(X)$ and $p_{bT_M(Z)}$ and p_b are the marginal densities of $T_M(Z)$ and Z , respectively. The solution to this optimization problem is given by the

optimal transport map T_m from $p_b(z|m)$ to the marginal $p_b(z)$. This is shown in Lemma 3 in Appendix B. Additionally, as our classifier $Z = h(X)$ is univariate, T_m has a closed-form solution given by $T_m(z) = F_z^{-1}(F_{z|m}(z))$ where F_z is the marginal cdf of $Z = h(X)$ and $F_{z|m}$ is the conditional cdf of Z given $M = m$ for $X \sim p_b$.

So, to estimate the optimal transport map T_m , we first need to estimate F_z , the marginal cdf of Z and $F_{z|m}$, the conditional cdf of Z given $M = m$, where $Z = h(X)$ is the classifier output on the background data X . To estimate F_z , we use the empirical cdf of the background data $h(X_i)$ to obtain an estimate $\hat{F}_z(t)$. Since we have sufficient background data, this is a good estimate of the marginal cdf.

Estimating the conditional cdf $F_{z|m}$ poses a more challenging task. We use a kernel conditional distribution estimator (using `npcdist` in R package `np` [Li and Racine, 2008, Hayfield and Racine, 2008, Li et al., 2013]) to estimate the conditional cdf. The challenge is that we need to find two optimal bandwidths for the kernel estimator, one along the z dimension and one along the m dimension. We note in our experiments that a fixed bandwidth works along the z dimension, however, the optimal bandwidth along the m dimension varies. Finding an adaptive optimal bandwidth w.r.t. M is computationally expensive. Instead, we take one of two approaches. The first approach is to assume that the optimal bandwidth along M changes as a step function of M , where the points at which it changes are visibly observable from the distribution of M . The second approach is to assume that a particular location-scale transformation of Z as a function of $\log(M)$ results in a constant optimal bandwidth for the kernel estimator of $F_{z|m}$. Specifically, we assume $\text{logit}(Z) = \mu(M) + \sigma(M)\epsilon$, where $\mu(M) = E[\text{logit}(Z)|\log(M)]$, $\sigma^2(M) = \text{Var}(\text{logit}(Z)|\log(M))$, and the conditional distribution estimator of $\epsilon|\log(M)$ has a fixed optimal bandwidth. The intuition behind taking the *logit* and log transformations comes

from the context of $Z = h(X)$ being a classifier output and the protected variable M usually being the invariant mass, which is a positively skewed variable in our experiments. Depending on the data set, the *logit* and log transformations may or may not be necessary.

Using this assumption, we estimate on the background data, $\widehat{\eta}_i = \text{logit}(h(X_i)) - \widehat{\mu}(M_i^X)$, where $\widehat{\mu}$ is an estimator of μ derived using non-parametric regression of $\text{logit}(h(X_i))$ on $\log(M_i^X)$. Then we can estimate $\widehat{\sigma}^2(M_i^X)$'s using a non-parametric regression of $\widehat{\eta}_i^2$ on $\log(M_i^X)$. Now, we can estimate ϵ using $\widehat{\epsilon}_i = \widehat{\eta}_i / \widehat{\sigma}(M_i^X)$ and estimate $F_{\epsilon|m}$ using a fixed-bandwidth conditional distribution estimator $\widehat{F}_{\epsilon|m}$. Then the conditional distribution of $Z|M^X$ can be derived as $F_{z|m}(t) = F_{\epsilon|m}((\text{logit}(t) - \mu(m))/\sigma(m))$. Therefore, $\widehat{F}_{z|m}(t) = \widehat{F}_{\epsilon|m}((\text{logit}(t) - \widehat{\mu}(m))/\widehat{\sigma}(m))$. The CDOT (Classifier Decorrelated via Optimal Transport) procedure is detailed in Algorithm 1 in Appendix B.

It is important to note that even though we call the classifier a decorrelated classifier in accordance with standard terminology in HEP, in reality the transformed classifier $T_M(h)$ is independent of M for the background data and not just uncorrelated. Second, the best approach to estimate the conditional distribution of $Z|M$ (specifically the optimal bandwidth along the m -axis) in Step 3 of Algorithm 1 in Appendix B, depends on the distribution of M and $Z|M$ for the background data. We can use the available background validation data to decide which approach is better for a particular dataset.

The optimal transport map $T_m(h)$ transports $p_b(z|m)$ to the marginal $p_b(z)$ for every fixed m . An additional contribution of this paper is to consider the optimal path or geodesic taken by the optimal transport map, i.e., to look at the intermediate steps of the transport problem. Let \mathcal{F} be the set of all distributions and $g_m : [0, 1] \rightarrow \mathcal{F}$ is such that $g_m(0) = p_b(\cdot|m)$ and $g_m(1) = p_b(\cdot)$. Then $\{g_m(t) : 0 \leq t \leq 1\}$ is a path connecting $p_b(z|m)$ and $p_b(z)$. The geodesic is the shortest path connecting $p_b(z|m)$ and $p_b(z)$ and it can be

shown that for the geodesic path, the transformation corresponding to an intermediate point in the path $g_m(t)$ is given by $th + (1 - t)T_m(h)$ [Villani, 2021]. Hence, the geodesic gives rise to a range of decorrelated classifiers with varying degrees of decorrelation.

2.2 Semi-parametric efficient test for signal detection

We propose an efficient test for the presence of a signal using only the protected variable M , which is usually the invariant mass. We assume that the support of its distribution, denoted by Ω , can be split into disjoint control and signal regions, denoted by \mathbb{C} and \mathbb{S} , respectively. Furthermore, we assume that the signal region is known. In the following, we rewrite the conditional mixture after the signal enrichment step, see eq. (2), streamlining the notation in order to simplify the presentation of this section. The model is:

$$M_1, \dots, M_n \stackrel{\text{iid}}{\sim} f(m) = (1 - \lambda) \cdot b(m) + \lambda \cdot s(m) \quad (3)$$

$$\text{s.t. } \text{support}(f) = \Omega = \mathbb{S} \cup \mathbb{C}, \quad \mathbb{S} \cap \mathbb{C} = \emptyset \quad \text{and} \quad \int_{\mathbb{S}} s(m) dm = 1$$

where $f(m) = q(m|Z > t)$ is the mixture density, $b(m) = p_b(m)$ is the background density, $s(m) = p_s(m|Z > t)$ is the signal density and $\lambda = \lambda_t = P(S = 1|Z > t)$ is the signal strength. Note that we have suppressed the dependence on the threshold t in all cases. The above is a semi-parametric model [van der Vaart, 1998, Kosorok, 2008] because the signal distribution is unknown (only its support is known), but the background is assumed to either be known or parametric. Throughout this section, we adopt the following conventions: if b denotes the background density, then $B(A)$ indicates its integral over the set A , i.e., $B(A) = \int_A b(x) dx$. Analogously, let $F_n(A) = n^{-1} \sum_{i=1}^n I(M_i \in A)$ be the integral with respect to the empirical distribution.

Formally, given n observations from the mixture in eq. (3), we propose a test that decides between the null hypothesis, i.e., no signal present $H_0 : \lambda = 0$, and the alternative

hypothesis $H_1 : \lambda > 0$. Recall that a test is a function of the data $\Psi : \Omega^n \rightarrow \{0, 1\}$ that returns 0 if it considers that the data does not provide evidence against the null and 1 otherwise. Furthermore, we say that a test Ψ_α is asymptotically valid at the α -level if it asymptotically controls the probability of choosing the alternative hypothesis when the null hypothesis is true by α , that is, $\lim_{n \rightarrow \infty} B(\Psi_\alpha(X_1, \dots, X_n) = 1) \leq \alpha$. Finally, the power of a test is the probability that chooses the alternative hypothesis when it is true, i.e. $F(\Psi_\alpha(X_1, \dots, X_n) = 1)$ where $\lambda > 0$ in eq. (3). All tests in this section are asymptotically powerful, in the sense that for a sample size large enough, they detect the alternative hypothesis. That is, for $\lambda > 0$, it follows that $\lim_{n \rightarrow \infty} F(\Psi_\alpha(X_1, \dots, X_n) = 1) = 1$.

To gain some insight, consider the case where the background b is known. It can be immediately observed that integrating the mixture density over the control region leads to the identification of the signal strength as a ratio between the probability of observing an event in the control region under the mixture and background distributions.

$$\lambda(F, B) = 1 - \frac{F(\mathbb{C})}{B(\mathbb{C})} = 1 - \frac{1 - F(\mathbb{S})}{1 - B(\mathbb{S})} \quad (4)$$

Replacing the mixture F by its empirical counterpart F_n leads to the plug-in estimator that compares the observed counts in the signal region to the expected background. This estimator is usually referred to as a counting experiment in the physics literature [Behnke et al., 2013]. In the following lemma, we establish that it is the semi-parametric efficient estimator of λ .

Lemma 1. *Under the model in eq. (3) with known background b , the plug-in estimator*

$$\lambda(F_n, B) = 1 - \frac{F_n(\mathbb{C})}{B(\mathbb{C})} \quad (5)$$

is the semiparametric efficient estimator, and it induces an asymptotic α -level test

$$\Psi_\alpha(F_n, B) = I(T(F_n, B) > z_{1-\alpha}) \text{ where } T(F_n, B) = \sqrt{n} \cdot \frac{F_n(\mathbb{S}) - B(\mathbb{S})}{\sqrt{F_n(\mathbb{S})(1 - F_n(\mathbb{S}))}} \quad (6)$$

and $z_{1-\alpha}$ is the $1 - \alpha$ quantile of the standard normal distribution.

The proof can be found in Appendix C.2. We remark that physicists do not usually know the exact boundaries of the signal region, but they expect the contribution of the signal in the control region to be small. Consider the case where an ϵ fraction of the signal leaks into the control region $\int_{\mathbb{C}} s(x) dx = \epsilon$. Furthermore, assume that the amount of contamination ϵ is smaller than the probability of observing an event from the background in the control region $B(\mathbb{C})$. Then, $\lambda(F_n, B)$ underestimates the signal strength

$$E[\lambda(F_n, B)] = \lambda \cdot \left[1 - \frac{\epsilon}{B(\mathbb{C})} \right] \quad (7)$$

Consequently, stronger contamination increases the bias of the signal strength estimator, which ultimately lowers the detection power of the test eq. (6), meaning that more observations are needed to detect the signal. Nevertheless, the test remains asymptotically valid since, under the null hypothesis, there can be no contamination.

Usually, researchers do not know the background distribution. Hence, one might be tempted to replace $T(F_n, B)$ in the test eq. (6) by the estimate $T(F_n, \hat{B})$ where \hat{B} is the plug-in estimator of the background obtained from a separate sample. However, the error term introduced by such replacement is not asymptotically negligible; see Appendix C.3. Fundamentally, this is due to the fact that the efficient estimator is robust to infinitesimal perturbations of the signal in the signal region rather than perturbations of the background. A natural next step is to consider the case where the background is parametric in eq. (3). That is, $b = b_\gamma$ s.t. $\gamma \in \mathbb{R}^K$. To avoid the data on the signal region severely affecting the estimation of the background, a natural idea is to fit the background using only observations in the control region. This intuition leads to the maximum likelihood estimator that censors

the signal region

$$(\gamma_*(F_n), \lambda_*(F_n)) = \arg \max_{\tilde{\gamma}, \tilde{\lambda}} \sum_{i=1}^n \ell(M_i, \tilde{\lambda}, \tilde{\gamma}) \text{ s.t. } B_\gamma(\Omega) = 1, \quad (8)$$

where $\ell(m, \lambda, \gamma) = I(m \in \mathbb{S}) \cdot \log((1 - \lambda) \cdot B_\gamma(\mathbb{S}) + \lambda) + I(m \in \mathbb{C}) \cdot \log((1 - \lambda) \cdot b_\gamma(m))$. The following lemma shows that this estimator is efficient when using a parametric background. The proof and the definition of $\tau_\lambda(F_n)$ are deferred to Appendix C.4

Lemma 2. *Under the model in eq. (3) with a parametric background, the censored MLE estimator in eq. (8) is efficient and induces an asymptotic α -level test*

$$\Psi_\alpha^{(K)}(F_n) = I\left(\sqrt{n} \cdot \frac{\lambda_*(F_n)}{\tau_\lambda(F_n)} > z_{1-\alpha}\right). \quad (9)$$

Although the censored MLE does not provide a closed-form solution for $\gamma_*(F_n)$, looking at the first order optimality condition for the signal strength reveals that the efficient estimator is analogous to eq. (5) but using the estimated parametric background $\lambda_*(F_n) = 1 - F_n(\mathbb{C})/B_{\gamma_*(F_n)}(\mathbb{C})$. Since the background is estimated from the data, there is a trade-off with respect to the size of the signal region. A small signal region can lead to part of the signal leaking into the control region, biasing the estimation of the background and ultimately biasing the signal strength estimator $\lambda_*(F_n)$. Conversely, a large signal region protects against the contamination of the control region, but it increases the variance of the background estimator due to reducing the amount of data in the control region in addition to making it harder to interpolate the background in the signal region. This, in turn, increases the variance of $\lambda_*(F_n)$. In both situations, the test based on $\lambda_*(F_n)$ remains valid, but it loses power, i.e., it requires more observations to detect the signal. Finally, it is worth noting that the censored MLE is equivalent to maximizing the conditional likelihood over the control region and extending it into the signal region, see Appendix C.7.

Note that if the parametric form is taken to be a truncated series, $b = b_\gamma = \sum_{k=1}^K \gamma_k \cdot \phi_k(x)$ where $\gamma \in \mathbb{R}^K$, an expectation-maximization algorithm [Dempster et al., 1977] can

be used to easily estimate the background parameters γ , see Appendix C.5. The resulting algorithm can be seen as a version of the D’Agostini iteration [Shepp and Vardi, 1982, D’Agostini, 1995] without binning the data. The binned version of the algorithm is commonly used in unfolding problems [Adye, 2011]. In our numerical studies, we use the K -th order Bernstein basis; see Appendix D.2 and in order to accelerate computations, we discretize the data using bins before estimating the censored MLE; see Appendix C.6.

3 Simulation studies

We investigate the performance of our method for the detection of high- p_T W bosons in Section 3.1, and of exotic high-mass resonance events in Section 3.2. In all experiments, the data is split into training, validation, and test datasets. The training data is used to fit a random forest classifier, however, one could use any probabilistic classifier. The validation data is used to perform decorrelation, calibrate the classifier, and calibrate the signal-enriched test to achieve a type I error of $\alpha = 0.05$. For further details see Appendix D.3.

Using the test dataset, we study the power of the signal-enriched test and the performance of the CDOT decorrelation algorithm. To analyze the power of the signal detection test, we proceed as follows: given a signal strength λ , we sub-sample $N = 500$ datasets of $n = 20000$ observations from the test dataset, such that $\lambda\%$ of those observations correspond to signal events. Then, for each dataset, we check if the test rejects the null hypothesis $H_0 : \lambda = 0$ and compute the empirical probability of rejecting the null hypothesis across datasets. For $\lambda = 0$, that probability is the empirical type-I error, while for $\lambda \in \{0.01, 0.02, 0.05\}$, it is the empirical power. In all cases, we report the empirical results with their corresponding Clopper–Pearson confidence intervals. Finally, to understand the utility of the decorrelation algorithm, we study the power of the signal-enriched test both

when using a non-decorrelated and decorrelated classifier to filter the observations.

3.1 Detection of high-p_T W bosons

In the following, we consider the identification of high-p_T W bosons, which is referred to as W-tagging. W-tagging is one of the benchmark experiments used to compare decorrelation methods in particle physics. In ATLAS [2018b], the ATLAS Collaboration performed a detailed study of some existing decorrelation methods for W-tagging. Here, we use the more recent W-tagging dataset from Kasieczka and Shih [2020] and Kitouni et al. [2021] to compare our proposed decorrelation method to existing methods.

The SM background process in the dataset consists of events where gluons and light-flavor quarks hadronize into jets (represented by $pp \rightarrow jj$), and the signal process consists of events with the SM production of two W-bosons (represented by $pp \rightarrow WW$), where both W-bosons decay into jets. The processes are simulated using Pythia 8.219 [Sjöstrand et al., 2008] with the condition that the initially produced particles have momentum $p_T > 250$ GeV. The detector responses are simulated using Delphes 3.4.1 [De Favereau et al., 2014], and the jets are reconstructed using FastJet 3.0.1 [Cacciari et al., 2012]. More details about the simulation can be found in Kasieczka and Shih [2020] and ATLAS [2018b]. The final selected dataset has jets that have mass $m \in [50, 300]$ GeV and momentum $p_T \in [300, 400]$ GeV. The protected variable is the invariant mass of the jets, which is scaled so that its range is $[0, 1]$. Table 1 in ATLAS [2018b] has a list of all the jet sub-structure variables that were used for training the auxiliary classifier.

The data in Kasieczka and Shih [2020] is split into training (background: 110k, signal: 250k), validation (background: 330k, signal: 80k) and test (background: 770k, signal: 80k) datasets. The training data is used to fit a random forest classifier with 1000 trees and a

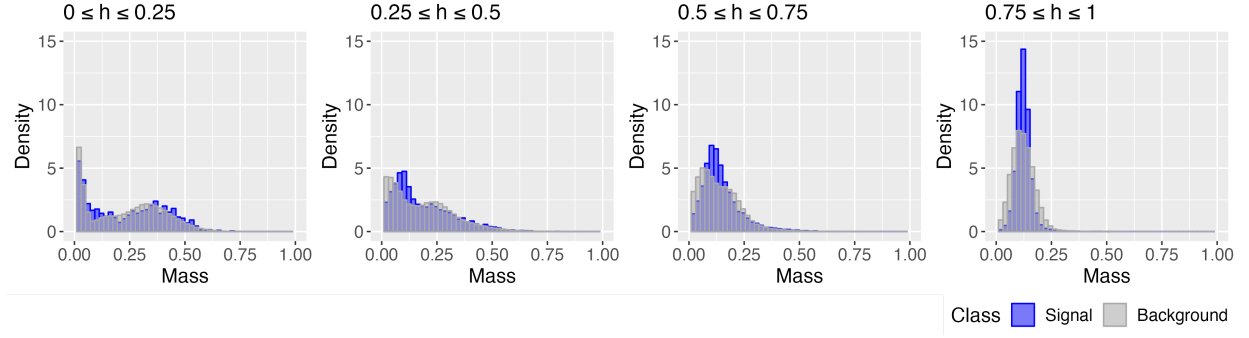


Figure 3: Density plots of the invariant mass for the W-tagging data for different ranges of the classifier output (h) without any decorrelation.

minimal node size of 800 samples. The validation data is used to train the CDOT algorithm (Algorithm 1 in Appendix B, using Approach 1) with splits set at $\{0.2, 0.4, 0.6\}$, i.e., a different fixed optimal bandwidth is chosen for each of the intervals $[0, 0.2]$, $[0.2, 0.4]$, $[0.4, 0.6]$, and $[0.6, 1]$ when training the kernel conditional distribution estimator.

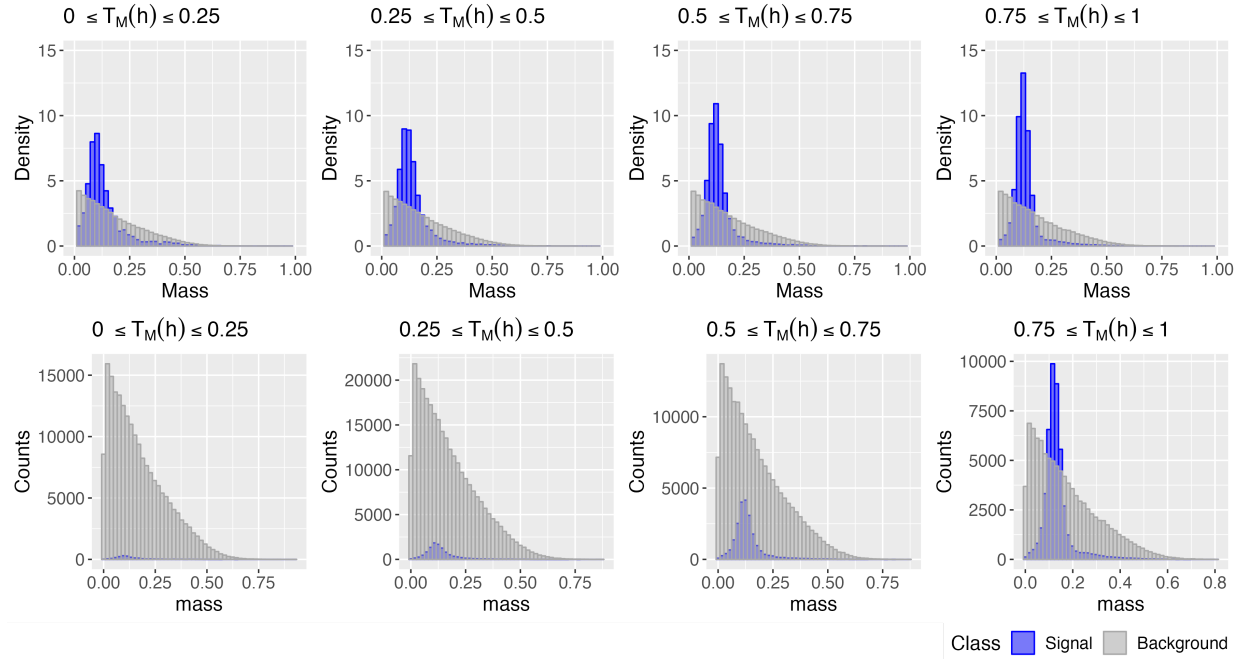


Figure 4: Post-decorrelation density plots (top) and histograms (bottom) of the invariant mass for the W-tagging data, for different ranges of the transformed classifier ($T_M(h)$).

Figure 3 shows the effect of sculpting on the background distribution when signal en-

richment is applied to the classifier output without any decorrelation. The background distribution demonstrates a bump as the classifier output (h) increases making it hard to detect the signal bump using a bump hunt. Figure 4 shows the distributions of both the background and the signal after decorrelating the classifier using CDOT, i.e., the signal enrichment cuts are now applied on the decorrelated classifier output ($T_M(h)$). As the decorrelated classifier output increases, the top row of the figure shows that the background distribution's shape remains the same avoiding sculpting. The bottom row further demonstrates the increase in the signal proportion.

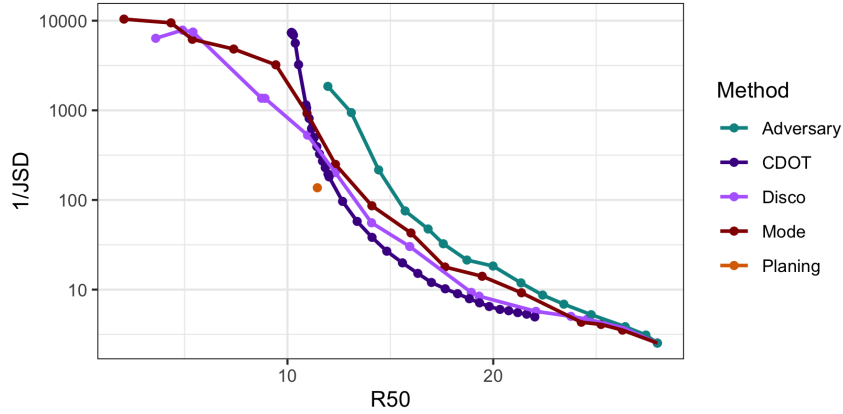


Figure 5: Decorrelation ($1/\text{JSD}$ on \log_{10} scale) versus background-rejection power ($R50$) plot comparing CDOT to existing decorrelation methods. The original plot without CDOT is taken from Figure 7 in Kitouni et al. [2021]

Figure 5 compares CDOT to state-of-the-art methods introduced in Section 1.2, namely, Disco, ANN, MoDe, and Planing [Chang et al., 2018]. We build on Figure 7 in Kitouni et al. [2021] by adding the performance of CDOT using the same metrics to the figure. The plot compares the methods on $1/\text{JSD}$ versus $R50$, where $R50$ is the background rejection power (inverse false positive rate) at 50% signal efficiency and JSD is the Jensen-Shannon divergence between the background observations that are above the cut at 50% signal efficiency and the background observations that are below the same cut. Higher $R50$ values

represent good classifier performance in separating the signal from the background and higher $1/\text{JSD}$ values represent higher decorrelation (independence) between the classifier and the protected variable for the background data. Figure 5 shows that while Disco and MoDe are able to achieve higher decorrelation scores at the expense of lower R50 values, looking at around $\text{R50} = 10$, we see that CDOT is able to achieve higher decorrelation scores for a higher amount of accuracy. The CDOT curve represents the performance of the intermediate classifiers given by the optimal transport geodesic. We see that by moving away from the fully decorrelated classifier, the drop in decorrelation is much faster than the gain in background-rejection power which suggests that it is recommended to use the fully decorrelated classifier for the bump hunt test. We also note that estimating $1/\text{JSD}$ is very sensitive to the selection of bins used to calculate it. We chose the same binning used in Kitouni et al. [2021] but changing the binning even slightly changes the $1/\text{JSD}$ scores.

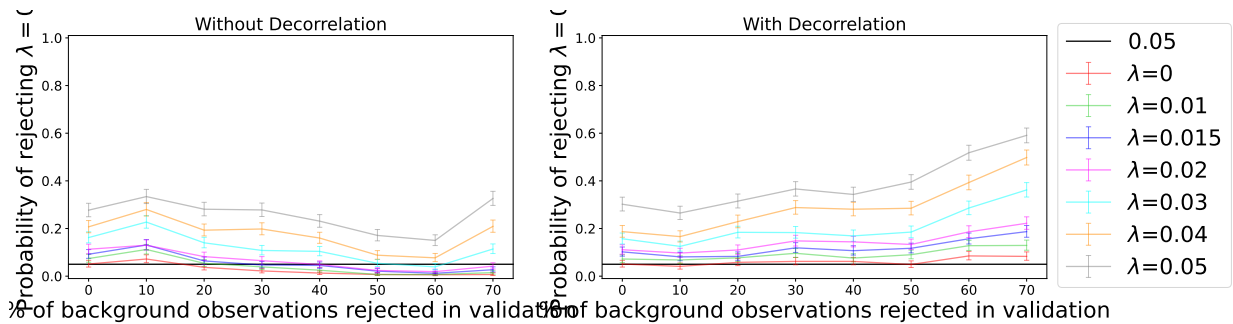


Figure 6: The type-I error rate ($\lambda = 0$) and power ($\lambda > 0$) analysis for the W-tagging test dataset. Clopper-Pearson intervals are shown for all estimates.

Regarding signal detection, using the model selection in eq. (100), we choose $K_* = 35$ as the best-calibrated test. Figures displaying the empirical type-I error and p-value plots can be found in Appendix D.4. Using the test dataset, we perform a power analysis of the test as the non-decorrelated and decorrelated classifiers are used to filter more data; see Figure 6. Figures 7 and 8 show one instance of the observed data and fitted background for

the original and decorrelated classifiers, respectively. Note that when sculpting is present, the estimated background includes a bump in the signal region. Hence, the signal-enriched tests that use the non-decorrelated classifier become more conservative, as shown by the near-zero type-I error rate in Figure 6, and lose power. Conversely, the signal-enriched test based on the decorrelated classifier avoids sculpting and approximately achieves the desired type-I error while improving its power as more data is filtered.

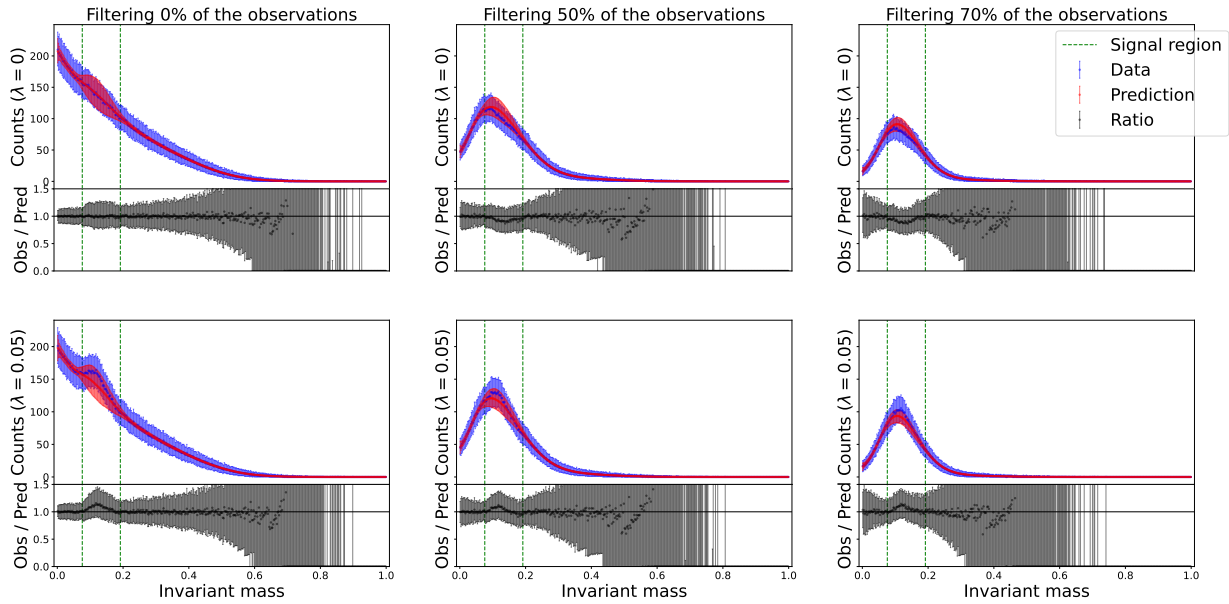


Figure 7: Background estimates for the W-tagging test dataset as more observations are filtered by the non-decorrelated classifier. First row corresponds to the null hypothesis (no signal). In the second row, 5% of the data comes from the signal distribution. Note the sculpting in the signal region. The intervals are 95% variability intervals based on 1000 simulations, and their midpoint is the median of the simulations.

3.2 Detection of exotic high-mass resonance events

We consider high-mass resonance events where an exotic high-mass particle is produced in proton-proton collisions and decays into two Higgs bosons. The two Higgs bosons individ-

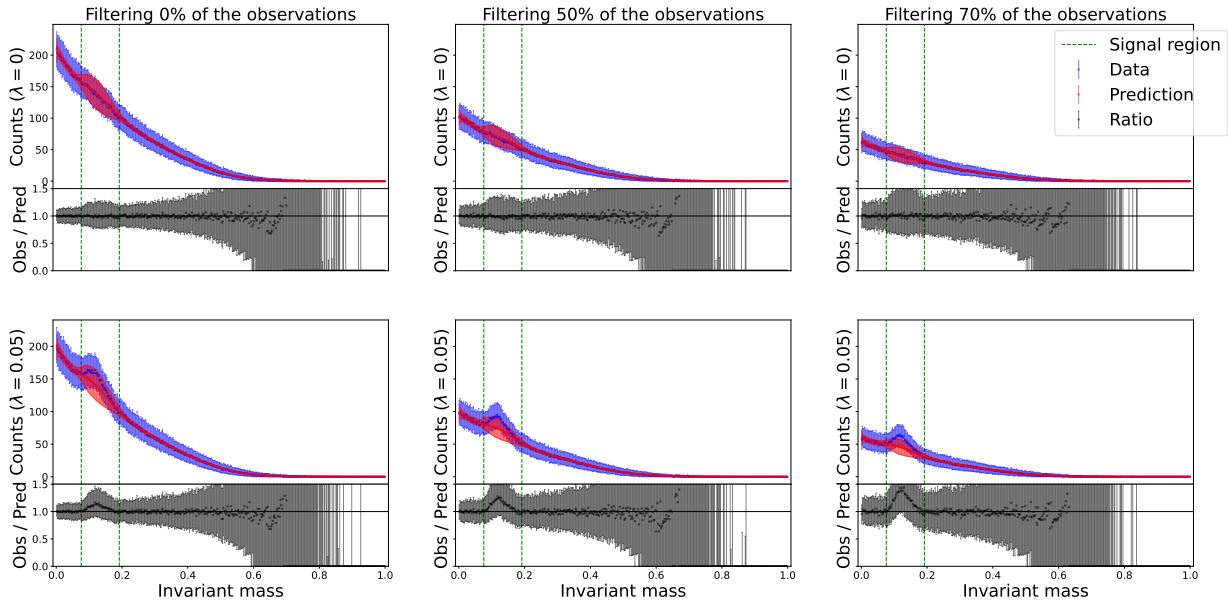


Figure 8: Background estimates for the W-tagging test dataset as more observations are filtered by the decorrelated classifier. Note that there is no sculpting. The intervals are 95% variability intervals based on 1000 simulations, and their midpoint is the median of the simulations.

ually then decay hadronically into two b-quarks, and so to detect the signal, we investigate events where four b-quarks are observed. This process is abbreviated as $X \rightarrow HH \rightarrow 4b$. The QCD background simulations are not entirely reliable for this final state, so we use this experiment to demonstrate the robustness of our entire pipeline to a misspecified background. We consider two kinds of background processes. The first is a “4b” background dataset that includes QCD multijet events that produce four b-quarks. The second is a “3b” background dataset consisting of events that have four jets, where exactly three are b-jets. The data was simulated using the MadGraph event generator software [Alwall et al., 2011] where the high-mass resonance was set to have invariant mass $m \approx 400$ GeV and selected events have all jets with momentum $p_T > 40$ GeV and jet pseudorapidity $|\eta| \leq 2.5$. The datasets contains 463,848 3b events, 62,993 4b events, and 44,196 signal events.

This was split into training data (3b: 50k, signal: 40k), validation data (3b: 120k) and test data ($3b \approx 294k$, $4b \approx 63k$, signal $\approx 4k$). The 3b and signal training data are used to fit a random forest classifier with 1000 trees and minimal node size as 100 samples. The 3b validation data is used to train CDOT Algorithm in Appendix B using Approach 2. The test data is used for evaluation of the decorrelation algorithm and the bump-hunting test. To check the robustness of our procedure to background misspecification, the classifier and CDOT training are performed on the 3b background and not the 4b background, whereas the test is performed on the 4b background. The kinematics of 3b events are similar, but not exactly the same, as those of 4b background events [CMS, 2022] and hence this is a good check of the robustness of the pipeline to moderate background misspecification.

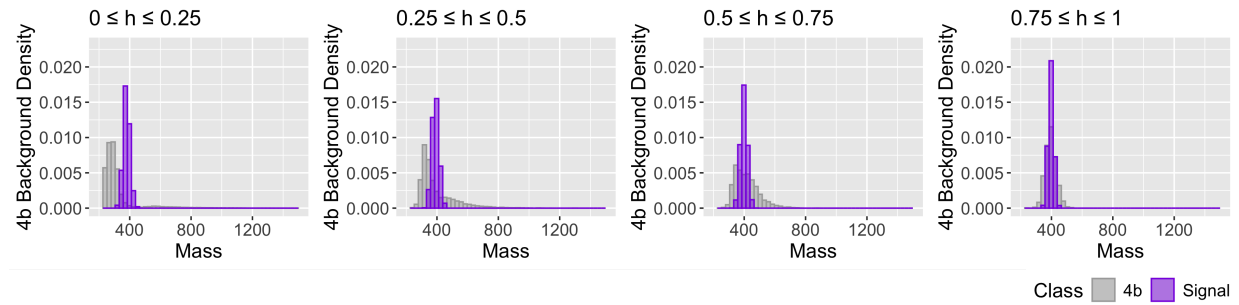


Figure 9: Density plots of the invariant mass for the 4b data set with signal, for different ranges of the classifier (h) without any decorrelation. We observe sculpting.

Figure 9 shows the effect of sculpting produced on the 4b background when signal enrichment is performed using the non-decorrelated classifier. In contrast, Figure 10 displays the distributions after decorrelating the classifier using CDOT. Note that even though CDOT is trained on just the 3b background, it is robust to decorrelating both the 3b test background as well as the 4b background.

Finally, we turn to signal detection. The proposed test, see eq. (9), depends on fitting the background with the Bernstein basis, see eq. (99), which is supported on the interval $[0, 1]$. Since the 3b and 4b data sets are not supported on the unit interval, we map them

to this interval. A visual inspection of the $3b$ background data in the validation dataset indicates that it decreases approximately exponentially. Thus, we transform all data in this section using the inverse CDF function of an exponential. Namely, given an observation, we apply the function $m \mapsto 1 - \exp\{-r \cdot (m - b)\}$, where b is the minimum invariant mass of the $3b$ validation background and $r = 0.003$, which provide an adequate fit to the data.

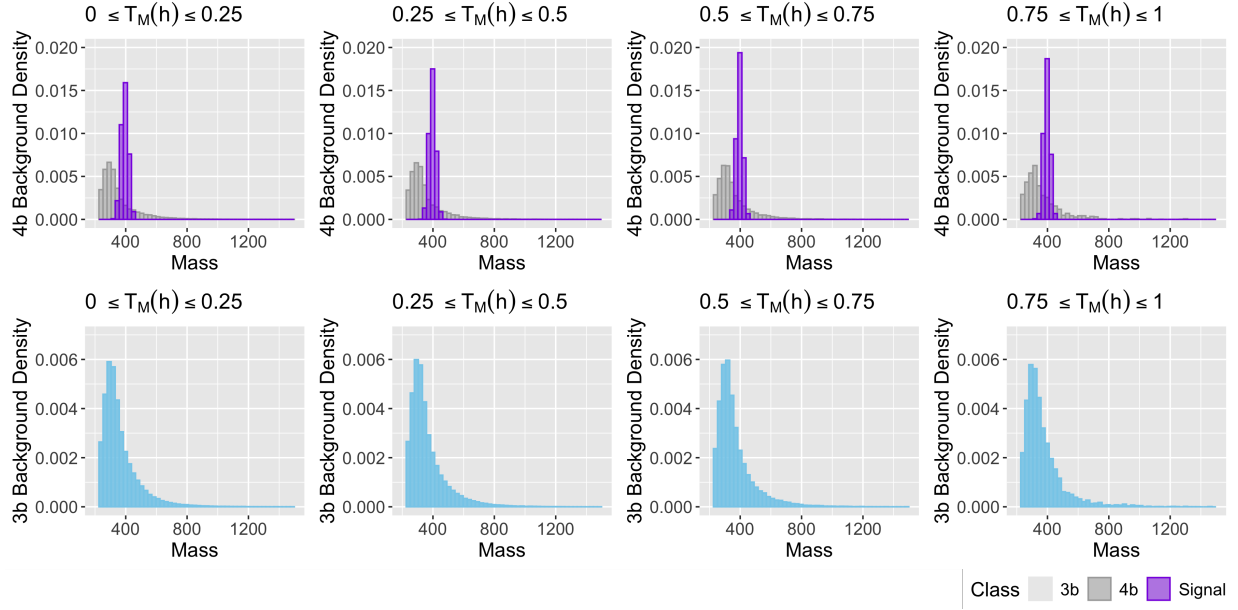


Figure 10: Post-decorrelation density plots of the invariant mass for the $4b$ data set with signal (top) and the test $3b$ background (bottom), for different ranges of the transformed classifier ($T_M(h)$). We see that CDOT trained on $3b$ avoids sculpting $4b$ as well as $3b$.

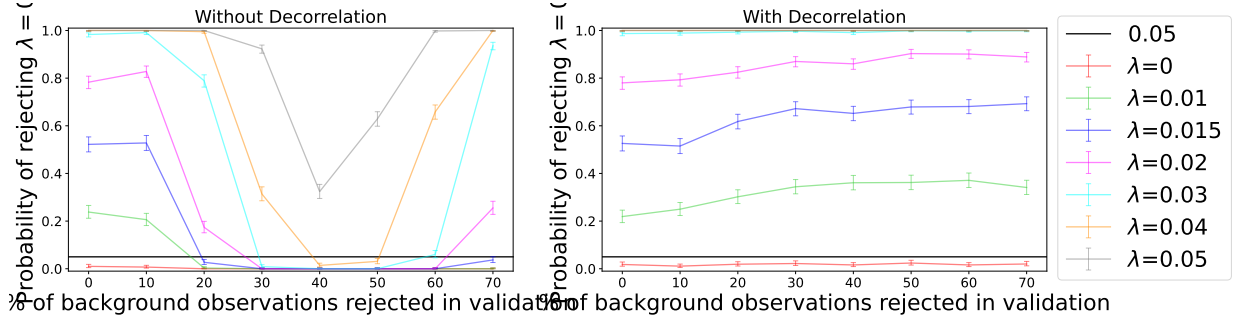


Figure 11: Validity and power analysis on the $3b$ test dataset.

Analogously to the previous analysis, using the $3b$ validation dataset we find that $K_* =$

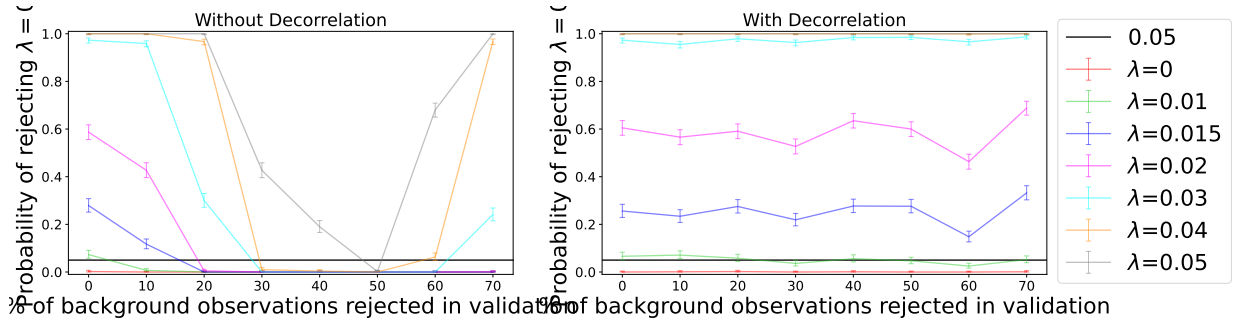


Figure 12: Validity and power analysis on 4b test dataset.

20 provides the best-calibrated test; the corresponding plots can be found in Appendix D.5. The power analysis with the 3b test dataset is shown in Figure 11, while the same analysis with the 4b test dataset is displayed in Figure 12. When there is no distribution shift between the validation and test datasets, the conclusions are similar to the previous section. The decorrelated classifier preserves the shape of background distribution; hence, the tests remain calibrated when enriched by a decorrelated classifier which increases their power. However, when there is a distribution shift between the validation and test datasets, we observe that the decorrelated classifier does not lead to an improvement in power, while the non-decorrelated classifier actually decreases the power. Importantly, all tests remain valid, albeit conservative, despite the background misspecification. Plots displaying the background estimation have been deferred to Appendix D.5.

4 Discussion

In this paper, we implemented the entire pipeline of signal detection in particle physics using bump hunting after performing signal enrichment using a decorrelated transformed classifier. We conclude from the experiments that both signal enrichment using cuts on a classifier as well as decorrelating the classifier before performing cuts improves the power of the bump hunt signal detection test. We also demonstrate in Section 3.2 that the bump

hunt test, as well as the decorrelation algorithm proposed in this paper, CDOT, are robust to some background model misspecification. In the future, it would be interesting to study the robustness of the procedures to different kinds of model misspecifications.

We note that CDOT, along with CNOTS [Algren et al., 2024], are post-processing decorrelation algorithms, meaning they can be applied to any pre-trained classifier to decorrelate it. The advantage of this is that we do not have to re-train the classifier again, lowering the computational cost of the whole procedure. It also has the advantage that domain experts can train a classifier for a particular application using their expert knowledge, and then use CDOT to decorrelate this pre-trained classifier. There may be some loss of signal detection power since we are optimizing the two problems, finding the optimal classifier and a decorrelated classifier, sequentially instead of together. From Section 3.1, it appears that CDOT compares favorably with existing state-of-the-art decorrelation methods.

Finally, we note that although in this work we focused on univariate protected variables, it is straightforward to extend the decorrelation algorithm to accommodate multivariate protected variables by changing the conditional density estimation to accommodate higher-dimensional conditioned variables. However, the proposed semi-parametric efficient test would have to be modified to use a multivariate score test as in Bickel et al. [2006].

Acknowledgments We thank Patrick Bryant for generating and providing the data for the exotic high-mass resonance detection experiment in Section 3.2. We also thank John Alison, Ben Nachman, David Shih, Sara Algeri, Tudor Manole, Kenta Takatsu, Lukas Heinrich, Tobias Golling, Malte Algren, Johnny Raine, Samuel Klein, the STAMPS research group at Carnegie Mellon University and the participants of *Systematic Effects and Nuisance Parameters in Particle Physics Data Analyses* workshop in Banff and *PHYSTAT - Statistics meets ML* at Imperial for useful discussions and comments on this work.

References

Tim Adye. Unfolding algorithms and tests using RooUnfold. In *PHYSTAT 2011*, Geneva, 2011. CERN.

Malte Algren, John Andrew Raine, and Tobias Golling. Decorrelation using optimal transport. *The European Physical Journal C*, 84(6), 2024.

Johan Alwall, Michel Herquet, Fabio Maltoni, Olivier Mattelaer, and Tim Stelzer. Madgraph 5: going beyond. *Journal of High Energy Physics*, 2011(6), 2011.

ATLAS. Identification of hadronically-decaying w bosons and top quarks using high-level features as input to boosted decision trees and deep neural networks in atlas at $\sqrt{s} = 13$ tev. Technical report, ATL-PHYS-PUB-2017-004, 2017a.

ATLAS. Performance of top quark and w boson tagging in run 2 with atlas. Technical report, ATLAS-CONF-2017-064, 2017b.

ATLAS. Observation of $H \rightarrow bb$ decays and VH production with the ATLAS detector. *Physics Letters B*, 786, 2018a.

ATLAS. Performance of mass-decorrelated jet substructure observables for hadronic two-body decay tagging in atlas. Technical report, ATL-PHYS-PUB-2018-014, 2018b.

ATLAS Collaboration. Search for New Particles in Two-Jet Final States in 7 TeV Proton-Proton Collisions with the ATLAS Detector at the LHC. *Physical Review Letters*, 105(16), October 2010.

Mark P Becker, Ilsoon Yang, and Kenneth Lange. EM algorithms without missing data. *Statistical Methods in Medical Research*, 6(1), 1997.

Olaf Behnke, Kevin Kröninger, Grégory Schott, and Thomas Schörner-Sadenius. *Data Analysis in High Energy Physics*. Wiley Online Library, 2013.

Peter J. Bickel, Ya'acov Ritov, and Thomas M. Stoker. Tailor-made tests for goodness of fit to semiparametric hypotheses. *The Annals of Statistics*, 34, 2006.

Patrick Bryant. *Search for Pair Production of Higgs Bosons in the Four Bottom Quark Final State Using Proton-Proton Collisions at $\sqrt{s} = 13$ Tev with the ATLAS Detector*.

PhD thesis, The University of Chicago, 2018.

Janice Button, George R. Kalbfleisch, Gerald R. Lynch, Bogdan C. Maglić, Arthur H. Rosenfeld, and M. Lynn Stevenson. Pion-pion interaction in the reaction $\bar{p} + p \rightarrow 2\pi^+ + 2\pi^- + n\pi^0$. *Physical Review*, 126(5), June 1962.

Matteo Cacciari, Gavin P Salam, and Gregory Soyez. Fastjet user manual: (for version 3.0. 2). *The European Physical Journal C*, 72:1–54, 2012.

CDF Collaboration. Global Search for New Physics with 2.0/fb at CDF. *Physical Review D*, 79(1), January 2009.

Spencer Chang, Timothy Cohen, and Bryan Ostdiek. What is the machine learning? *Phys. Rev. D*, 97:056009, March 2018.

Taoli Cheng, Jean-François Arguin, Julien Leissner-Martin, Jacinthe Pilette, and Tobias Golling. Variational autoencoders for anomalous jet tagging. *Physical Review D*, 107(1):016002, 2023.

Georgios Choudalakis. On hypothesis testing, trials factor, hypertests and the Bum-pHunter, January 2011.

CMS. Observation of higgs boson decay to bottom quarks. *Physical review letters*, 121(12), 2018.

CMS. Search for higgs boson pair production in the four b quark final state in proton-proton collisions at $\sqrt{s} = 13$ tev. *arXiv preprint arXiv:2202.09617*, 2022.

Jack H. Collins, Kiel Howe, and Benjamin Nachman. Extending the Bump Hunt with Machine Learning. *Physical Review D*, 99(1), January 2019.

Glen Cowan, Kyle Cranmer, Eilam Gross, and Ofer Vitells. Asymptotic formulae for likelihood-based tests of new physics. *The European Physical Journal C*, 71(2), February 2011.

Giulio D'Agostini. A multidimensional unfolding method based on bayes' theorem. *Nuclear Instruments and Methods in Physics Research Section A: Accelerators, Spectrometers, Detectors and Associated Equipment*, 362(2-3), 1995.

J De Favereau, Christophe Delaere, Pavel Demin, Andrea Giammanco, Vincent Lemaitre, Alexandre Mertens, and Michele Selvaggi. Delphes 3: a modular framework for fast simulation of a generic collider experiment. *Journal of High Energy Physics*, 2014(2): 1–26, 2014.

A. P. Dempster, N. M. Laird, and D. B. Rubin. Maximum Likelihood from Incomplete Data Via the EM Algorithm. *Journal of the Royal Statistical Society: Series B (Methodological)*, 39(1), 1977.

Biagio Di Micco, Maxime Gouzevitch, Javier Mazzitelli, and Caterina Vernieri. Higgs boson potential at colliders: Status and perspectives. *Reviews in Physics*, 5:100045, 2020.

James Dolen, Philip Harris, Simone Marzani, Salvatore Rappoccio, and Nhan Tran. Thinking outside the rocs: Designing decorrelated taggers (ddt) for jet substructure. *Journal of High Energy Physics*, 2016(5), 2016.

Lyndon Evans and Philip Bryant. LHC machine. *Journal of instrumentation*, 3(08), 2008.

Subhashis Ghosal. Convergence rates for density estimation with Bernstein polynomials. *The Annals of Statistics*, 29(5), 2001.

Eilam Gross and Ofer Vitells. Trial factors for the look elsewhere effect in high energy physics. *The European Physical Journal C*, 70(1-2), November 2010.

Philip Coleman Harris, Dylan Sheldon Rankin, and Cristina Mantilla Suarez. An approach to constraining the Higgs width at the LHC and HL-LHC. *arXiv preprint arXiv:1910.02082*, 2019.

Tristen Hayfield and Jeffrey S Racine. Nonparametric econometrics: The np package. *Journal of statistical software*, 27, 2008.

Gregor Kasieczka and David Shih. Disco fever: Robust networks through distance correlation. *arXiv preprint arXiv:2001.05310*, 2020.

Gregor et al. Kasieczka. The LHC Olympics 2020: A Community Challenge for Anomaly Detection in High Energy Physics. *Reports on Progress in Physics*, 84(12), December 2021.

Ouail Kitouni, Benjamin Nachman, Constantin Weisser, and Mike Williams. Enhancing searches for resonances with machine learning and moment decomposition. *Journal of High Energy Physics*, 2021(4):1–23, 2021.

Samuel Klein and Tobias Golling. Decorrelation with conditional normalizing flows. *arXiv preprint arXiv:2211.02486*, 2022.

Michael R. Kosorok. *Introduction to Empirical Processes and Semiparametric Inference*. Springer, New York, 2008. ISBN 978-0-387-74977-8 978-0-387-74978-5.

S. Kullback and R. A. Leibler. On Information and Sufficiency. *The Annals of Mathematical Statistics*, 22(1), 1951.

Qi Li and Jeffrey S Racine. Nonparametric estimation of conditional cdf and quantile functions with mixed categorical and continuous data. *Journal of Business & Economic Statistics*, 26(4), 2008.

Qi Li, Juan Lin, and Jeffrey S Racine. Optimal bandwidth selection for nonparametric conditional distribution and quantile functions. *Journal of Business & Economic Statistics*, 31(1), 2013.

George G Lorentz. *Bernstein polynomials*. American Mathematical Soc., 2013.

Gilles Louppe, Michael Kagan, and Kyle Cranmer. Learning to pivot with adversarial networks. *Advances in neural information processing systems*, 30, 2017.

Louis Lyons. Open statistical issues in Particle Physics. *The Annals of Applied Statistics*, 2(3), 2008.

Tudor Manole, Patrick Bryant, John Alison, Mikael Kuusela, and Larry Wasserman. Background modeling for double higgs boson production: Density ratios and optimal transport. *arXiv preprint arXiv:2208.02807*, 2022.

Eric A Moreno, Thong Q Nguyen, Jean-Roch Vlimant, Olmo Cerri, Harvey B Newman, Avikar Periwal, Maria Spiropulu, Javier M Duarte, and Maurizio Pierini. Interaction

networks for the identification of boosted $h \rightarrow bb$ decays. *Physical Review D*, 102(1), 2020.

Ian Moult, Benjamin Nachman, and Duff Neill. Convolved substructure: analytically decorrelating jet substructure observables. *Journal of High Energy Physics*, 2018(5), 2018.

Gigi Rolandi. LHC results - Highlights. *arXiv preprint arXiv:1211.3718*, 2012.

Lawrence A Shepp and Yehuda Vardi. Maximum likelihood reconstruction for emission tomography. *IEEE transactions on medical imaging*, 1(2), 1982.

Chase Shimmin, Peter Sadowski, Pierre Baldi, Edison Weik, Daniel Whiteson, Edward Goul, and Andreas Søgaard. Decorrelated jet substructure tagging using adversarial neural networks. *Physical Review D*, 96(7):074034, 2017.

Torbjörn Sjöstrand, Stephen Mrenna, and Peter Skands. A brief introduction to pythia 8.1. *Computer Physics Communications*, 178(11):852–867, 2008.

A. W. van der Vaart. *Asymptotic Statistics*. Cambridge University Press, 1998.

Cédric Villani. *Topics in optimal transportation*, volume 58. American Mathematical Soc., 2021.

SUPPLEMENTARY MATERIAL

A Further introduction to the problem

A.1 Introduction to the detection of exotic high-mass resonance

For the second example, we study the production of a high-mass resonance where an exotic high-mass particle decays into two Higgs bosons. The Higgs boson is an unstable particle that decays roughly within 10^{-22} seconds, making it impossible to directly detect it. Instead, the SM predicts that the Higgs boson decays into a pair of bottom quarks (b-quarks) 60% of the time, experimentally shown by ATLAS [2018a] and CMS [2018], which can be used to detect the original resonance. To detect this, one needs to investigate the events where four b-quarks are observed and detect in which events the four b-quarks originate from the resonance (signal events) versus events where the four b-quarks were produced by a different process (background events). The background process is dominated by jet production via strong interactions of quarks and gluons from the colliding protons. The b-quarks themselves hadronize to form streams of other particles and their final stable decay products can be reconstructed in the detectors as so-called b-jets. The kinematic properties of the four b-jets (e.g., momentum, energy, angles, etc.) can then be used to detect if a particular event is likely to be a high-mass resonance event. Similar to W-boson production, the invariant mass can also be used to identify signal events from background events.

The distribution of the signal, in this case, can be approximated accurately; however, simulating the background distribution, in this case, suffers from being computationally intractable due to the presence of large higher-order perturbative corrections in strong

interactions [Di Micco et al., 2020]. Previous research has assumed that there are auxiliary events that are related to the background distribution via a distributional shift and can be used to estimate the background distribution [Bryant, 2018, Manole et al., 2022]. An example of such auxiliary events would be events that result in less than four b-quarks, making them impossible to have come from a signal event, but having similar kinematic properties as the background [Bryant, 2018]. Since the background distribution is now being estimated, the background samples might not be entirely accurate, and hence, similar to W-boson production, a signal detection test based on a classifier trained on these samples might be affected.

A.2 Flowchart of the method

The entire proposed pipeline of the signal detection process in the paper is demonstrated in Figure 13. During the implementation, we split the simulated background data into a training data set and a validation data set, where the training data set is used to train the probabilistic classifier and the validation data set is used to train the decorrelation algorithm. We train a random forest classifier as the probabilistic classifier h that separates the signal from the background. However, one could use any pre-trained probabilistic classifier and decorrelate it for the background using the decorrelation algorithm presented here.

B Derivation and implementation of CDOT

In this section, we show that the transformed classifier we need in Section 2.1 is given by the optimal transport map from the conditional density $p_b(z|m)$ to $p_b(z)$, where $Z = h(X)$, $X \sim p_b$, and M is the protected variable.

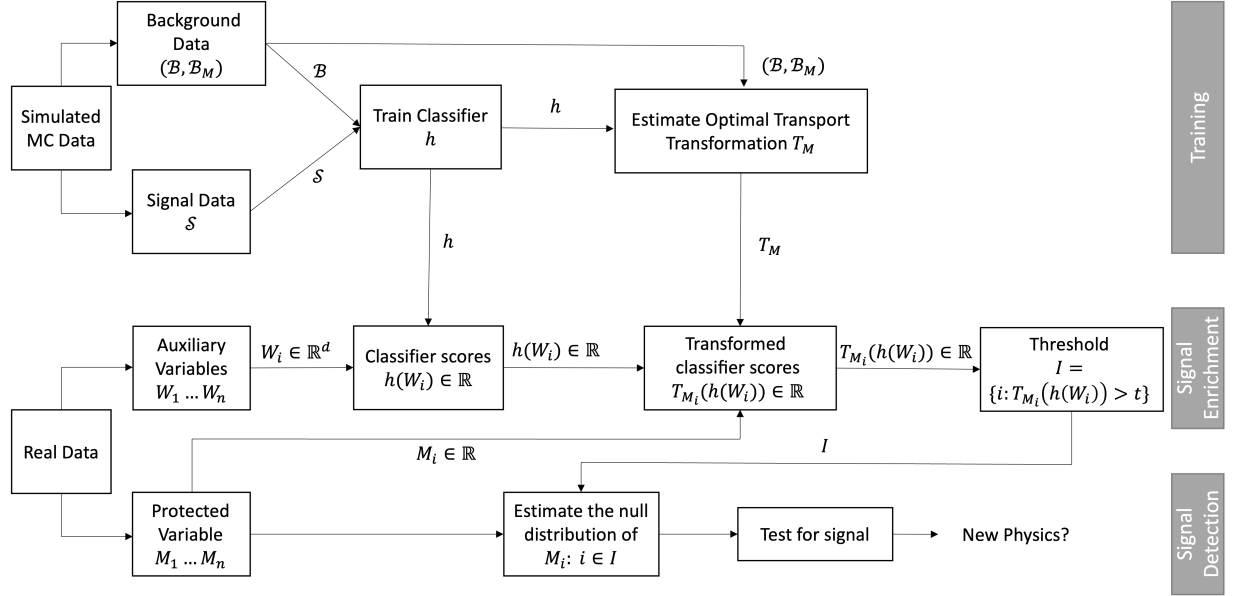


Figure 13: Flowchart of the signal detection process. The process can be divided into three stages - training, signal enrichment, and signal detection stages. In the training stage, we use the Monte Carlo (MC) simulated background and signal data to train the supervised classifier h as well as the optimal transport map T_M to get the classifier decorrelated through optimal transport (CDOT), $T_M(h(\cdot))$. In the signal enrichment stage, we threshold the trained CDOT on the real experimental data. Finally, in the signal detection stage, we use the protected variable for the selected real data to perform bump-hunt signal detection.

Lemma 3. *Given any two random variables (Z, M) , a map that minimizes*

$$\mathbb{E} [|T_M(Z) - Z|^2] \quad (10)$$

subject to $T_M(Z)$ independent of M and $T_M(Z)$ has the same marginal distribution as Z , is given by the optimal transport map T_m from $F_{z|m}$ to F_z under the ℓ^2 cost function, where $F_{z|m}$ and F_z are the cdfs of $Z|M$ and Z respectively.

Proof: Let T_m denote the optimal transport map from $F_{z|m}$ to F_z , then by definition T_m minimizes $\mathbb{E} [c(Z, T_M(Z))|M = m]$ for each m and $P(T_m(Z) \leq t|M = m) = F_z(t)$, where

$c(x, y)$ is the cost function. Now let $f_m(Z)$ be any other map such that given $M = m$, $f_m(Z)$ is distributed as F_z , that is, $P(f_m(Z) \leq t | M = m) = F_z(t)$. Then, by definition, when the cost function is the ℓ^2 loss, $c(x, y) = \|x - y\|^2$,

$$\mathbb{E} [\|T_m(Z) - Z\|^2 | M = m] dP(m) \leq \mathbb{E} [\|f_m(Z) - Z\|^2 | M = m] dP(m) \quad (11)$$

Then

$$\mathbb{E} [\|T_m(Z) - Z\|^2] = \int \mathbb{E} [\|T_m(Z) - Z\|^2 | M = m] dP(m) \quad (12)$$

$$\leq \int \mathbb{E} [\|f_m(Z) - Z\|^2 | M = m] dP(m) = \mathbb{E} [\|f_m(Z) - Z\|^2]. \quad (13)$$

This shows that $T_m(Z)$ is independent of M , its marginal distribution is F_z and it minimizes $\mathbb{E}[\|T_m(Z) - Z\|^2]$ among all such maps. Notice that in this result, M or Z can be of any dimension since the dimension does not enter in the argument.

In our case where we make the classifier output $Z = h(X)$ independent of M , the form of the optimal transport map from $F_{z|m}$ to F_z when $h(X)$ and M are one-dimensional is derived by observing that by definition,

$$\begin{aligned} F_z(T_m(t)) &= P(T_m(Z) \leq T_m(t) | M = m) = F_{z|m}(t) \\ \implies T_m(t) &= F_z^{-1}(F_{z|m}(t)). \end{aligned}$$

We remark that an alternative approach is to choose $T_m(z)$ such that M is independent of $T_M(Z)$ and such that the Wasserstein distance between (Z, M) and $(T_M(Z), M)$ is minimized. The solution in this case is to define $T_m(z)$ to be the optimal transport map from $F_{z|m}$ to B where B is the barycenter, that is, the distribution that minimizes $\int W^2(F_{z|m}, B) dP(m)$.

The CDOT (Classifier Decorrelated via Optimal Transport) procedure is detailed below:

Algorithm 1. CDOT decorrelated classifier output on the experimental data \mathcal{E} .

Input: $X_i \in \mathcal{B}$ (*Training:* \mathcal{B}_1 , *Validation:* \mathcal{B}_2), $Y_j \in \mathcal{S}, W_k \in \mathcal{E}, M_i^X, M_j^Y, M_k \forall i, j, k$.

Output: $T_{M_k}(h(W_k))$, decorrelated classifier output for every k .

1. Train a probabilistic classifier h on $X_i \in \mathcal{B}_1, Y_j \in \mathcal{S} \forall i, j$, which gives the probability of being a signal event given the data.
2. Evaluate $h(X_i), h(Y_j), h(W_k) \forall i, j, k$.
3. Estimate the conditional distribution $F_{z|m}$ for $X_i \in \mathcal{B}_2$ ($Z = h(X)$) using one of the two approaches.

(a) Approach 1:

- i. Choose splits in the range of M , $\{m_0, m_1, \dots, m_l\}$.
- ii. For each split $i \in \{1, \dots, l\}$, estimate $\widehat{F}_{z|m}^{(i)}$ using a kernel conditional distribution estimator with fixed optimal bandwidths on $Z_j = h(X_j)$ and M_j^X for $X_j \in \mathcal{B}_2$ such that $m_{i-1} \leq M_j^X \leq m_i$.
- iii. Then for the experimental data,

$$\widehat{F}_{z|m}(h(W_k)) = \widehat{F}_{z|m}^{(i)}(h(W_k)) \text{ if } m_{i-1} \leq M_k \leq m_i \quad (14)$$

(b) Approach 2:

- i. Estimate $\widehat{\mu}(M_i^X) = \widehat{\mathbb{E}} [\logit(h(X_i)) | \log(M_i^X)]$ (non-parametric regression).
- ii. Evaluate $\widehat{\eta}_i = \logit(h(X_i)) - \widehat{\mu}(M_i^X)$.
- iii. Estimate $\widehat{\sigma}^2(M_i^X) = \widehat{\mathbb{E}} [\widehat{\eta}_i^2 | \log(M_i^X)]$ (non-parametric regression).
- iv. Evaluate $\widehat{\epsilon}_i = \widehat{\eta}_i / \widehat{\sigma}(M_i^X)$.
- v. Estimate $\widehat{F}_{\epsilon|m}$ using a kernel conditional distribution estimator with a fixed optimal bandwidth on ϵ_i 's given $\log(M_i^X)$'s.

vi. Then for the experimental data,

$$\widehat{F}_{z|m}(h(W_k)) = \widehat{F}_{\epsilon|m} [(logit(h(W_k)) - \widehat{\mu}(M_k)) / \widehat{\sigma}(M_k)] \quad (15)$$

4. Estimate $\widehat{F}_z(t)$ using the empirical CDF estimator on the background data \mathcal{B}_2 .

5. Evaluate the CDOT classifier output as $T_{M_k}(h(W_k)) = \widehat{F}_z^{-1}(\widehat{F}_{z|m}(h(W_k)))$.

Note that all the kernel conditional distribution (CCDF) estimators were obtained using the `npcdist` function in the R package `np` [Li and Racine, 2008, Hayfield and Racine, 2008, Li et al., 2013]. The fixed optimal bandwidths in both approaches above were chosen using the least-squares cross-validation method of Li and Racine [2008] and Li et al. [2013].

C Signal detection in the density model

C.1 CLT for Z-estimators

The following lemma is an informal version of the asymptotic normality theorem for Z-estimators presented in section 5.3 of van der Vaart [1998]. We refer the reader to it for the specific regularity conditions needed. It should be noted that the result does not require probability measures to have a density. Hence, we use $\int g \, dF$ to denote that we integrate the function g with respect to the measure F .

Lemma 4. *Let $\theta(F)$ be the parameters that satisfies the following zero equation*

$$\int h(x, \theta(F)) \, dF(x) = 0. \quad (16)$$

Let F_n denote the empirical distribution. Then

$$\sqrt{n}(\theta(F_n) - \theta(F)) \xrightarrow{d} \mathcal{N}(0, \tau^2(F)) \quad (17)$$

$$\text{where } \tau^2(F) = \int \psi^2(F, x) dF(x) \quad (18)$$

$$\text{and } \psi(F, x) = - \left[\int \frac{\partial h}{\partial \theta}(x, \theta(F)) dF(x) \right]^\dagger \cdot h(x, \theta(F)) \quad (19)$$

Consider a coordinate λ of θ . Then

$$\sqrt{n} \left(\frac{\theta_\lambda(F_n) - \theta_\lambda(F)}{\sqrt{[\tau^2(F_n)]_{\lambda, \lambda}}} \right) \xrightarrow{d} \mathcal{N}(0, 1). \quad (20)$$

C.2 Efficient estimator with known background

Lemma 1. Under the model in eq. (3) with known background b , the plug-in estimator

$$\lambda(F_n, B) = 1 - \frac{F_n(\mathbb{C})}{B(\mathbb{C})} \quad (5)$$

is the semiparametric efficient estimator, and it induces an asymptotic α -level test

$$\Psi_\alpha(F_n, B) = I(T(F_n, B) > z_{1-\alpha}) \text{ where } T(F_n, B) = \sqrt{n} \cdot \frac{F_n(\mathbb{S}) - B(\mathbb{S})}{\sqrt{F_n(\mathbb{S})(1 - F_n(\mathbb{S}))}} \quad (6)$$

and $z_{1-\alpha}$ is the $1 - \alpha$ quantile of the standard normal distribution.

Proof. The score function for λ is $g = (s - b)/f$. Consider the parametric submodel $f_t = (1 - \lambda)b + \lambda s(1 + t \cdot h)$ where h is supported on the signal region \mathbb{S} , and it is mean zero w.r.t. the signal. The nuisance tangent set is

$$\Lambda = \left\{ \frac{h \cdot s}{f} : \exists h \in \mathbb{H} \right\} \text{ where } \mathbb{H} = \left\{ h : \int h \cdot s = 0 \text{ and } \int_{\mathbb{S}} h = 1 \right\}. \quad (21)$$

The orthogonal projection of g onto Λ is given by

$$\Pi g = \inf_{h \in H} \left\| g - \frac{hs}{f} \right\|_2^2 = \frac{f}{s} \left[g - \frac{B(\mathbb{C})}{F(\mathbb{S})} \right] \cdot I_{\mathbb{S}}. \quad (22)$$

The efficient score g_* is g minus its projection onto Λ :

$$g_* = g - \Pi g = \frac{B(\mathbb{C})}{F(\mathbb{S})} \cdot I_{\mathbb{S}} - \frac{1}{1-\lambda} \cdot I_{\mathbb{C}}. \quad (23)$$

The efficient estimator is defined as the following z-estimator

$$\sum_{i=1}^n g_*(X_i, \hat{\lambda}) = 0 \implies \hat{\lambda} = 1 - \frac{F_n(\mathbb{C})}{B(\mathbb{C})}. \quad (24)$$

The efficient influence function is

$$\psi(F, x) = \left[- \int \frac{\partial g_*}{\partial \lambda} f \right]^{-1} g_*(x) \quad (25)$$

$$= \frac{F(\mathbb{S})(1-\lambda)}{B(\mathbb{C})} \left[\frac{B(\mathbb{C})}{F(\mathbb{S})} \cdot I(x \in \mathbb{S}) - \frac{I(x \in \mathbb{C})}{1-\lambda} \right] \quad (26)$$

$$= (1-\lambda) \cdot I(x \in \mathbb{S}) - \frac{F(\mathbb{S})}{B(\mathbb{C})} \cdot I(x \in \mathbb{C}) \quad (27)$$

and its variance is

$$\tau^2(F) = \int \psi^2(F, x) f(x) = (1-\lambda)^2 F(\mathbb{S}) + \frac{F^2(\mathbb{S})}{B(\mathbb{C})} (1-\lambda) \quad (28)$$

$$= (1-\lambda) \frac{F(\mathbb{S})}{B(\mathbb{C})}. \quad (29)$$

The asymptotic variance of $\hat{\lambda}$ is τ^2 , verifying that it is efficient. We then have the following central limit theorem

$$\sqrt{n} \left(\frac{\lambda(F_n, B) - \lambda(F, B)}{\tau(F_n)} \right) \xrightarrow{d} \mathcal{N}(0, 1). \quad (30)$$

Under the null hypothesis,

$$\sqrt{n} \cdot \frac{\lambda(F_n, B)}{\tau(F_n)} \xrightarrow{d} \mathcal{N}(0, 1) \quad (31)$$

and consequently

$$\Psi_\alpha(F_n, B) = I(T(F_n, B) > Z_{1-\alpha}) \quad (32)$$

$$\text{where } T(F_n, B) = \sqrt{n} \cdot \frac{\lambda(F_n, B)}{\tau(F_n)} = \sqrt{n} \cdot \frac{F_n(\mathbb{S}) - B(\mathbb{S})}{\sqrt{F_n(\mathbb{S})(1 - F_n(\mathbb{S}))}} \quad (33)$$

is an asymptotic α -level test. \square

C.3 Impossibility of replacing known background by plug-in estimator

The following lemma states that to replace the known background under the null hypothesis, we must have $|\hat{B}(\mathbb{C}) - B(\mathbb{C})| = o_p(n^{-1})$. However, this is not achievable even when given an auxiliary sample from the background unless excessively constraining assumptions are placed on the background.

Lemma 5. *Assume that the background mass in the control region is bounded away from zero*

$$\exists c > 0 \text{ s.t. } c < \min \{B(\mathbb{C}), 1 - B(\mathbb{C})\} \quad (34)$$

and that \hat{B} is an estimator of the true background that does not depend on F_n . It follows that for $\Psi_\alpha(F_n, \hat{B})$ to be an asymptotic $1-\alpha$ test, it must hold that $|\hat{B}(\mathbb{C}) - B(\mathbb{C})| = o_p(n^{-1})$

Proof. Recall that

$$\Psi_\alpha(F_n, B) = I(T(F_n, B) > z_{1-\alpha}) \quad (35)$$

Let \hat{B} be an estimator of B , we have that $T(F_n, \hat{B}) = T(F_n, B) + R$ where $R = T(F_n, B) - T(F_n, \hat{B})$. The first term converges to a standard normal. Hence, if the remainder converges faster to zero, i.e., $R = o_p(n^{-1/2})$, under the null hypothesis, it follows that $T(F_n, \hat{B})$ converges to a standard normal. Consequently, $\Psi_\alpha(F_n, \hat{B})$ is an asymptotically valid test.

Note that

$$|R| = |T(F_n, B) - T(F_n, \hat{B})| = n^{1/2} \cdot \frac{|\hat{B}(\mathbb{S}) - B(\mathbb{S})|}{\sqrt{F_n(\mathbb{S}) \cdot (1 - F_n(\mathbb{S}))}} \quad (36)$$

Under the null, it holds by the weak law of large numbers that

$$F_n(\mathbb{S}) \xrightarrow{\text{P}} B(\mathbb{S}) \quad (37)$$

Hence, since $0 < B(\mathbb{C}) < 1$, it follows by the continuous mapping theorem that

$$\sqrt{\frac{F_n(\mathbb{S}) \cdot (1 - F_n(\mathbb{S}))}{B(\mathbb{S}) \cdot (1 - B(\mathbb{S}))}} \xrightarrow{\text{P}} 1 \quad (38)$$

Consequently, $|T(F_n, B) - T(F_n, \hat{B})| = o_p(n^{-1/2})$ is implied by

$$|\hat{B}(\mathbb{C}) - B(\mathbb{C})| = o_p\left(\frac{\sqrt{B(\mathbb{C}) \cdot (1 - B(\mathbb{C}))}}{n}\right) \quad (39)$$

Since $B(\mathbb{C})$ is bounded away from zero and one, the condition is implied by $|\hat{B}(\mathbb{C}) - B(\mathbb{C})| = o_p(n^{-1})$. \square

C.4 Efficient estimator with parametric background

Lemma 2. *Under the model in eq. (3) with a parametric background, the censored MLE estimator in eq. (8) is efficient and induces an asymptotic α -level test*

$$\Psi_\alpha^{(K)}(F_n) = I\left(\sqrt{n} \cdot \frac{\lambda_*(F_n)}{\tau_\lambda(F_n)} > z_{1-\alpha}\right). \quad (9)$$

Proof. The score function is $g = (g_\lambda, g_\gamma)$ where

$$g_\lambda = (b_\gamma - s)/f \quad (40)$$

$$g_\gamma = \frac{1-\lambda}{f} \cdot \frac{\partial b}{\partial \gamma} \quad (41)$$

Consider the sub-parametric model $f_t = (1-\lambda) \cdot b_\gamma + \lambda \cdot s \cdot (1 + t \cdot h)$ where h is supported on the signal region \mathbb{S} and it's mean zero w.r.t. the signal. That is, the nuisance tangent set is defined by

$$\Lambda = \left\{ \frac{h \cdot s}{f} : \exists h \in \mathbb{H} \right\} \text{ where } \mathbb{H} = \left\{ h : \int h \cdot s = 0 \text{ and } \int_{\mathbb{S}} h = 1 \right\} \quad (42)$$

The orthogonal projection of g onto Λ is given by

$$\Pi g = \inf_{h \in H} \left\| g - \frac{hs}{f} \right\|_2^2 = \left[g - \frac{E[g \cdot I_{\mathbb{S}}]}{F(\mathbb{S})} \right] I_{\mathbb{S}} \quad (43)$$

consequently, we obtain the efficient score by projecting to the orthogonal complement of Λ

$$g^* = g - \Pi g = g \cdot I_{\mathbb{C}} + \frac{E[g \cdot I_{\mathbb{S}}]}{F(\mathbb{S})} I_{\mathbb{S}} \quad (44)$$

where

$$g_\lambda^* = \frac{B_\gamma(\mathbb{C})}{(1-\lambda)B_\gamma(\mathbb{S}) + \lambda} \cdot I_{\mathbb{S}} - \frac{1}{1-\lambda} \cdot I_{\mathbb{C}} \quad (45)$$

$$g_\gamma^* = \frac{1-\lambda}{(1-\lambda)B_\gamma(\mathbb{S}) + \lambda} \cdot \left(\int_{\mathbb{S}} \frac{\partial b_\gamma}{\partial \gamma} \right) \cdot I_{\mathbb{S}} + \frac{\partial b_\gamma}{\partial \gamma} \cdot \frac{1}{b_\gamma} \cdot I_{\mathbb{C}} \quad (46)$$

Then, the estimands of interest are

$$(\lambda_*(F), \gamma_*(F)) \text{ s.t. } \int g^*(x, \lambda_*(F), \gamma_*(F)) \cdot f(x) dx = 0 \quad (47)$$

that correspond to the following M -estimand

$$(\lambda_*(F), \gamma_*(F)) = \arg \max_{\tilde{\gamma}, \tilde{\lambda}} \int \ell(x, \tilde{\lambda}, \tilde{\gamma}) \cdot f(x) dx \text{ s.t. } B_\gamma(\Omega) = 1 \quad (48)$$

$$\text{where } \ell(x, \lambda, \gamma) = I(x \in \mathbb{S}) \cdot \log((1-\lambda)B_\gamma(\mathbb{S}) + \lambda) + I(x \in \mathbb{C}) \cdot \log((1-\lambda)b_\gamma(x)) \quad (49)$$

The efficient estimators are the corresponding plug-in estimators $(\lambda_*(F_n), \gamma_*(F_n))$. It is worth noting that the efficient estimator for the signal strength is the same as the efficient estimator with known background but replacing the known background for the estimated parametric background

$$\lambda_*(F_n) = 1 - \frac{F_n(\mathbb{C})}{B_{\gamma_*(F_n)}(\mathbb{C})} \quad (50)$$

However, there is no closed-form solution for the background parameters $\gamma_*(F_n)$. Thus, we propose an expectation-maximization Dempster et al. [1977] algorithm to solve for them in appendix C.5.

Regarding inference, by lemma 4, it follows that the efficient influence function is

$$\psi(F, x) = \left[\int \frac{\partial^2 \ell}{\partial \theta \partial \theta}(x, \theta_*(F)) \cdot f(x) dx \right]^\dagger \cdot \frac{\partial \ell}{\partial \theta}(x, \theta_*(F)) \text{ where } \theta_*(F) = (\lambda_*(F), \gamma_*(F)) \quad (51)$$

and its variance is $\tau^2(F) = \int \psi(F, x) \cdot \psi^t(F, x) \cdot f(x) dx$. Furthermore, let $\tau_\lambda(F_n) = \sqrt{\tau_{\lambda,\lambda}^2(F_n)}$. It follows by lemma 4 that

$$\sqrt{n} \left(\frac{\lambda_*(F_n) - \lambda}{\tau_\lambda(F_n)} \right) \xrightarrow{d} \mathcal{N}(0, 1) \quad (52)$$

Finally, under the null hypothesis, we have that $\lambda = 0$, and consequently the following is an asymptotic $1 - \alpha$ level test

$$\Psi_\alpha(F_n) = I(T(F_n) > Z_{1-\alpha}) \quad (53)$$

$$\text{where } T(F_n) = \sqrt{n} \cdot \frac{\lambda_*(F_n)}{\tau_\lambda(F_n)} \quad (54)$$

□

C.5 Expectation-Maximization for censored MLE

Henceforth, assume that the parametric background is given by a truncated series

$$b = b_\gamma = \sum_{k=1}^K \gamma_k \cdot \phi_k(x), \text{ where } \gamma \in \mathbb{R}^K, \quad (55)$$

and recall the censored MLE estimator

$$(\gamma_*(F_n), \lambda_*(F_n)) = \arg \max_{\gamma, \lambda} \sum_{i=1}^n \ell(M_i, \lambda, \gamma) \text{ s.t. } B_\gamma(\Omega) = 1 \quad (56)$$

where the loss censors the signal region

$$\ell(m) = I(m \in \mathbb{S}) \cdot \log((1 - \lambda) \cdot (1 - B_\gamma(\mathbb{C})) + \lambda) + I(m \in \mathbb{C}) \cdot \log((1 - \lambda) \cdot b_\gamma(m)) \quad (57)$$

In the following let $n_{\mathbb{S}}$ denote the number of observations in the signal region $n_{\mathbb{S}} = \sum_{i=1}^n I(M_i \in \mathbb{S})$, and $n_{\mathbb{C}} = n - n_{\mathbb{S}}$ denote the number of observations in the control region.

The above optimization doesn't have a closed-form solution, but the first-order optimality conditions indicate that the solution satisfies the following equalities

$$\lambda_*(F_n) = 1 - \frac{F_n(\mathbb{C})}{B_{\gamma_*(F_n)}(\mathbb{C})} , \quad B_{\gamma_*(F_n)}(\Omega) = 1 \quad (58)$$

$$\text{and } \frac{B_{\gamma_*(F_n)}(\mathbb{C})}{F_n(\mathbb{C})} \cdot \phi_k(\mathbb{C}) = \frac{1}{n} \sum_{i=1}^n I(x_i \in \mathbb{C}) \cdot \frac{\phi_k(M_i)}{b_{\gamma_*(F_n)}(M_i)} \quad \text{for } 1 \leq k \leq K \quad (59)$$

In the following, we will see that we can use an Expectation-Maximization (EM) approximation [Dempster et al., 1977] to obtain an iterative algorithm that converges to solutions that satisfy the above equations. In particular, we will use the methodology push-forward by Becker et al. [1997], which approximates the origin loss function by an EM-like loss without using an statistical argument.

We start by introducing a guess for the solution of γ at the q th iteration

$$\max_{\gamma: B_\gamma(\Omega)=1} \sum_{i=1}^n \ell(M_i) = \max_{\lambda, \gamma: B_\gamma(\Omega)=1} n_{\mathbb{S}} \cdot \log((1-\lambda) \cdot (1 - B_\gamma(\mathbb{C})) + \lambda) + n_{\mathbb{C}} \cdot \log(1-\lambda) \quad (60)$$

$$+ \sum_{i=1}^n I(M_i \in \mathbb{C}) \cdot \log \left(\sum_{k=1}^K \gamma_k \cdot \phi_k(X_i) \cdot \frac{\gamma_k^{(q)} \cdot b_{\gamma^{(q)}}(M_i)}{\gamma_k^{(q)} \cdot b_{\gamma^{(q)}}(M_i)} \right) \quad (61)$$

Then, noting that $b_\gamma^{(q)}(M_i) = \sum_{k=1}^K \gamma_k^{(q)} \cdot \phi_k(M_i)$, we lower-bound the objective via Jensen's inequality

$$\max_{\lambda, \gamma: B_\gamma(\Omega)=1} n_{\mathbb{S}} \cdot \log((1-\lambda) \cdot (1 - B_\gamma(\mathbb{C})) + \lambda) + n_{\mathbb{C}} \cdot \log(1-\lambda) \quad (62)$$

$$+ \sum_{k=1}^K \sum_{i=1}^n I(M_i \in \mathbb{C}) \cdot \frac{\gamma_k^{(q)} \cdot \phi_k(M_i)}{b_{\gamma^{(q)}}(M_i)} \cdot \log \left(\frac{\gamma_k \cdot b_{\gamma^{(q)}}(M_i)}{\gamma_k^{(q)}} \right) \quad (63)$$

Finally, we remove the terms that are constant w.r.t. the optimization

$$\max_{\lambda, \gamma: B_\gamma(\Omega)=1} n_{\mathbb{S}} \cdot \log((1-\lambda) \cdot (1 - B_\gamma(\mathbb{C})) + \lambda) + n_{\mathbb{C}} \cdot \log(1-\lambda) \quad (64)$$

$$+ \sum_{k=1}^K a_k \cdot \gamma_k^{(q)} \cdot \log(\gamma_k) \quad (65)$$

where

$$a_k = \sum_{i=1}^n I(M_i \in \mathbb{C}) \cdot \frac{\phi_k(M_i)}{b_{\gamma^{(q)}}(M_i)} \quad (66)$$

Let $(\lambda^{(q+1)}, \gamma^{(q+1)})$ denote the solution of the above system of equations. It follows that the solution must satisfy the following conditions

$$\lambda^{(q+1)} = 1 - \frac{F_n(\mathbb{C})}{B_{\gamma^{(q+1)}}(\mathbb{C})} \quad , \quad B_{\gamma^{(q+1)}}(\Omega) = 1 \quad (67)$$

and

$$\text{for } 1 \leq k \leq K \quad \gamma_k^{(q+1)} = \gamma_k^{(q)} \cdot \frac{1 - B_{\gamma^{(q+1)}}(\mathbb{C}) + \frac{\lambda^{(q+1)}}{1-\lambda^{(q+1)}}}{n_S} \cdot \frac{a_k}{\phi_k(\mathbb{C})} \quad (68)$$

$$= \gamma_k^{(q)} \cdot \frac{B_{\gamma^{(q+1)}}(\mathbb{C})}{F_n(\mathbb{C})} \cdot \frac{1}{\phi_k(\mathbb{C})} \cdot \frac{a_k}{n} \quad (69)$$

Solving the system of equations leads to a normalized D'Agostini iteration [Shepp and Vardi, 1982, D'Agostini, 1995] for $\gamma^{(q+1)}$ that doesn't depend on $\lambda^{(q+1)}$

$$\gamma_k^{(q+1)} = \frac{\tilde{\gamma}_k}{B_{\tilde{\gamma}}(\Omega)} \quad \text{where} \quad \tilde{\gamma}_k = \gamma_k^{(q)} \cdot \frac{a_k}{\phi_k(\mathbb{C})} \quad (70)$$

Finally, note that at the fix point γ_∞ , eqs. (67) and (68) become eq. (58). Since eq. (56) is concave w.r.t. γ , the iteration converges to the unique maximizer. Ergo, $\gamma^{(\infty)} = \gamma_*(F_n)$, and consequently $\lambda^{(\infty)} = \lambda_*(F_n)$.

C.6 Discretized censored MLE

An issue when implementing the efficient test in the continuous case eq. (53), is to obtain a stable and fast implementation of the influence function eq. (51), which requires the inversion of the empirical Hessian. In order to sidestep this issue, we discretize the data and rely on the discrete delta method to construct or asymptotically valid test. Henceforth, assume that the parametric background is given by a truncated series eq. (55) and discretize

the density model eq. (3). That is, we partition the control region into L bins and take the whole signal region as one bin. Namely, define the disjoint sets

$$\mathbb{C} = \cup_{l=1}^L \mathbb{C}_l \text{ s.t. } \mathbb{C}_i \cap \mathbb{C}_j = \emptyset \text{ for } i \neq j \quad (71)$$

and their corresponding counts

$$n_{\mathbb{S}} = n \cdot F_n(\mathbb{S}) \text{ and } n_l = n \cdot F_n(\mathbb{C}_l) \text{ for } 1 \leq l \leq L \quad (72)$$

The counts follow a Multinomial distribution

$$(n_1, \dots, n_L, n_{\mathbb{S}}) \sim \text{Multinomial}(n_C, p) \text{ where } p_l = (1 - \lambda)B_{\gamma}(\mathbb{C}_l) \text{ for } 1 \leq l \leq L \quad (73)$$

$$p_{\mathbb{S}} = (1 - \lambda)B_{\gamma}(\mathbb{S}_l) + \lambda \quad (74)$$

Let $\mathbb{F}_n(\mathbb{C})$ denote the estimated probabilities in the control region

$$\mathbb{F}_n(\mathbb{C}) = \left[F_n(\mathbb{C}_1), \dots, F_n(\mathbb{C}_L) \right]^t \quad (75)$$

The discretized censored maximum likelihood estimator is

$$(\gamma_*(F_n), \lambda_*(F_n)) = \arg \max_{\gamma, \lambda} \ell(\mathbb{F}_n(\mathbb{C}), \lambda, \gamma) \text{ s.t. } B_{\gamma}(\Omega) = 1 \quad (76)$$

where

$$\ell(\mathbb{F}_n(\mathbb{C}), \lambda, \gamma) = (1 - F_n(\mathbb{C})) \cdot \log((1 - \lambda) \cdot (1 - B_{\gamma}(\mathbb{C})) + \lambda) \quad (77)$$

$$+ F_n(\mathbb{C}) \cdot \log(1 - \lambda) \quad (78)$$

$$+ \sum_{l=1}^L F_n(\mathbb{C}_l) \cdot \log(B_{\gamma}(\mathbb{C}_l)) \quad (79)$$

Following an analogous EM-approximation as in section appendix C.5, we can derive the following D'Agostini iteration that converges to $\gamma_*(F_n)$

$$\gamma_k^{(q+1)} = \frac{\tilde{\gamma}_k}{B_{\tilde{\gamma}}(\Omega)} \text{ where } \tilde{\gamma}_k = \gamma_k^{(q)} \cdot \frac{a_k}{\phi_k(C)} \text{ and } a_k = \sum_{l=1}^L F_n(\mathbb{C}_l) \cdot \frac{\phi_k(\mathbb{C}_l)}{B_{\gamma^{(q)}}(\mathbb{C}_l)} \quad (80)$$

Note that the above iteration is the natural discretization of the continuous iteration eq. (70). Finally, $\lambda_*(F_n)$ can still be computed by the ratio between observed to expected counts $\lambda_*(F_n) = 1 - \frac{F_n(\mathbb{C})}{B_{\gamma^*(F_n)}(\mathbb{C})}$.

Noting that $\lambda_*(F_n)$ is only a function of the counts in the control region, we can proceed analogously to appendix C.5 and obtain a central limit by the discrete delta method. Let $\mathbb{F}(\mathbb{C})$ denote the population vector of probabilities in the control region

$$\mathbb{F}(\mathbb{C}) = \left[F(\mathbb{C}_1), \dots, F(\mathbb{C}_L) \right] \quad (81)$$

it follows by the central limit theorem that

$$\sqrt{n} \cdot (\mathbb{F}_n(\mathbb{C}) - \mathbb{F}(\mathbb{C})) \xrightarrow{\text{d}} \mathcal{N}(0, D) \quad (82)$$

where $D \in \mathbb{R}^{(L-1) \times (L-1)}$, $D_{l,l} = F(\mathbb{C}_l) \cdot (1 - F(\mathbb{C}_l))$ and $D_{l,j} = -F(\mathbb{C}_l) \cdot F(\mathbb{C}_j)$ for $j \neq l$.

Thus, by the discrete delta method and Slutsky's theorem, we have that

$$\sqrt{n} \cdot \frac{\lambda_*(F_n) - \lambda_*(F)}{\sqrt{g(F_n)^t \cdot D_n \cdot g(F_n)}} \xrightarrow{\text{d}} \mathcal{N}(0, 1) \quad (83)$$

where $g(F_n) = \nabla_{\mathbb{F}_n(\mathbb{C})} \lambda_*(F_n)$ is the gradient with respect to the empirical probabilities, and D_n is the empirical covariance matrix of the probabilities $D_n \in \mathbb{R}^{(L-1) \times (L-1)}$, $[D_n]_{l,l} = F_n(\mathbb{C}_l) \cdot (1 - F_n(\mathbb{C}_l))$ and $[D_n]_{l,j} = -F_n(\mathbb{C}_l) \cdot F_n(\mathbb{C}_j)$ for $j \neq l$.

Finally, analogously to the efficient test in the continuous case eq. (53), we define our asymptotic $1 - \alpha$ level test to be

$$\Psi_\alpha(F_n) = I(T(F_n) > Z_{1-\alpha}) \quad (84)$$

$$\text{where } T(F_n) = \sqrt{n} \cdot \frac{\lambda_*(F_n)}{\sqrt{g(F_n)^t \cdot D_n \cdot g(F_n)}} \quad (85)$$

C.7 Equivalence between censored and conditional MLE

Consider the mixture model eq. (3) where the background is known to belong to the set \mathcal{B} . Since the signal vanishes in the control region, it follows that the conditional distribution

of the mixture on the control region depends only on the background distribution

$$M|M \in C \sim \frac{f(m)}{F(\mathbb{C})} \cdot I(m \in \mathbb{C}) = \frac{b(m)}{B(\mathbb{C})} \cdot I(m \in \mathbb{C}) \quad (86)$$

A natural idea is to estimate the conditional background distribution on the control region, and then extend it to the signal region, that is, to force the estimated background to integrate to one on the whole domain. This is justified if there is a unique way of extending the conditional background, and consequently the conditional measure identifies the measure on the whole domain. For instance, this is the case when the true background distribution is known to be a polynomial.

Proposition 1 (Polynomial densities that agree on \mathbb{C} must agree on Ω). *Let \mathcal{B} be some set of densities supported on Ω such that $b \in \mathcal{B}$ and for any $\tilde{b} \in \mathcal{B}$ it holds that*

$$(0) \tilde{b} \text{ is a polynomial, } \tilde{b} \geq 0 \text{ and } \tilde{B}(\Omega) = 1 \quad (87)$$

Furthermore, consider the function $d(f, g)$ in $\mathcal{B} \times \mathcal{B}$ such that

$$(1) d(f, f) = 0 \quad (2) d(f, g) = 0 \implies f = g \text{ a.e.} \quad (3) d(f, g) \geq 0 \quad \forall f, g \in \mathcal{B} \quad (88)$$

then

$$b = \arg \min_{\tilde{b} \in \mathcal{B}} d(b, \tilde{b}) = \arg \min_{\tilde{b} \in \mathcal{B}} d\left(\frac{b}{B(C)} \cdot I_{\mathbb{C}}, \frac{\tilde{b}}{\tilde{B}(C)} \cdot I_{\mathbb{C}}\right) \quad (89)$$

The lemma allows us to rewrite the signal strength as a function of F by exploiting the equivalence in equation eq. (89). Namely,

$$\lambda^*(F) = 1 - \frac{F(\mathbb{C})}{B_F^*(\mathbb{C})} \text{ where } b_F^* = \arg \min_{\tilde{b} \in \mathcal{B}} d\left(\frac{f}{F(\mathbb{C})} \cdot I_{\mathbb{C}}, \frac{\tilde{b}}{\tilde{B}(\mathbb{C})} \cdot I_{\mathbb{C}}\right) \quad (90)$$

Furthermore, consider using the Kullback-Leibler divergence [Kullback and Leibler, 1951] for d , then we obtain the conditional maximum likelihood estimator

$$\lambda^*(F_n) = 1 - \frac{F_n(\mathbb{C})}{B_{F_n}^*(\mathbb{C})} \quad (91)$$

where

$$b_{F_n}^* = \arg \max_{\tilde{b} \in \mathcal{B}} \sum_{i=1}^n I(M_i \in \mathbb{C}) \cdot \log \left(\frac{\tilde{b}(M_i)}{\tilde{B}(\mathbb{C})} \right) \text{ s.t. } \tilde{B}(\Omega) = 1 \quad (92)$$

Note that the condition $\tilde{B}(\Omega) = 1$ guarantees the valid extension of the conditional density to the whole domain.

Finally, regardless of the uniqueness of the extended background, both the conditional and censored MLE coincide from an algorithmic point of view. Recall the censored maximum likelihood estimator is given by

$$(\lambda^*(F_n), b_{F_n}^*) = \arg \max_{\tilde{\lambda}, \tilde{b} \in \mathcal{B}: \tilde{B}(\Omega)=1} n_{\mathbb{S}} \cdot \left((1 - \tilde{\lambda}) \cdot (1 - \tilde{B}(\mathbb{C})) + \tilde{\lambda} \right) \quad (93)$$

$$+ \sum_{i=1}^n I(M_i \in \mathbb{C}) \cdot \log \left((1 - \tilde{\lambda}) \cdot \tilde{b}(M_i) \right) \quad (94)$$

The first order optimality condition for λ_* is given by eq. (91). Plugging the result back into the optimization eq. (93) gives us the conditional MLE objective eq. (92).

Proof of proposition 1. Since $b \in \mathcal{B}$, by (1) and (3), it follows that the minimum must be achieved

$$d\left(\frac{b}{B(\mathbb{C})} \cdot I_{\mathbb{C}}, \frac{b^*}{B^*(\mathbb{C})} \cdot I_{\mathbb{C}}\right) = 0 \quad (95)$$

by (2), we know that the function must agree a.e. on the control region

$$\frac{b}{B(\mathbb{C})} = \frac{b^*}{B^*(\mathbb{C})} \text{ a.e. } x \in \mathbb{C} \quad (96)$$

by (0), we can extend the previous equation to all the domain

$$\frac{b}{B(\mathbb{C})} = \frac{b^*}{B^*(\mathbb{C})} \text{ a.e. } x \in \Omega \quad (97)$$

Integrating to both sides over Ω , and using the fact that $\tilde{B}(\Omega) = 1$ for all $\tilde{b} \in \mathcal{B}$, we get

$$B(\mathbb{C}) = B^*(\mathbb{C}) \quad (98)$$

and consequently $b = b^*$ a.e. $x \in \Omega$

□

D Simulation details

D.1 Code

The code to reproduce the experiments can be accessed at

<https://github.com/lkania/cdot>

D.2 Bernstein basis

In our numerical studies, we use the K th order Bernstein basis

$$\phi_k(x) = \binom{K}{k} \cdot x^k \cdot (1-x)^{K-k} \text{ for } 0 \leq x \leq 1 \quad (99)$$

while restricting the parameters γ to be non-negative $\gamma_k \geq 0 \forall k$ and satisfy $\sum_{k=0}^K \gamma_k = K + 1$. These restrictions guarantee that b_γ is a density function. Polynomials in Bernstein form have been routinely used in high-energy physics for background modeling [Rolandi, 2012, Harris et al., 2019] since they uniformly approximate any continuous function on Ω at a rate of $O(1/\sqrt{K})$ [Lorentz, 2013] and do not suffer from boundary bias [Ghosal, 2001]. Furthermore, in order to accelerate computations, we discretize the data using bins before estimating the censored MLE, see Appendix C.6.

D.3 Calibration of signal-enriched test

In all experiments, the data is split into training, validation, and test datasets. The training background and signal samples are used to fit a supervised probabilistic classifier. Let $h : \mathcal{X} \rightarrow [0, 1]$ denote the trained classifier. Conditioned on the training dataset, the classifier is a deterministic function that maps each observation to a score, with higher scores indicating that an event is more likely to be a signal event.

The validation dataset is used for three purposes. First, if performing decorrelation, the validation data is used to train the decorrelation algorithm by finding the optimal transport map, $T_M(h)$, on the validation background data. Note that if decorrelation is not used, the transport map is defined as the identity map $T_M(h) = h$. Second, the validation dataset and the transformed classifier output are used to find the cut-off point that filters $t\%$ of the background samples. To do this, we compute the score $T_M(h)$ of all background observations and find their t -th quantile, denoted by $q(t)$. Thus, the indicator function $I(T_M(h(X)) \geq q(t))$ filters $t\%$ of the background observations in the validation dataset. Third, the validation dataset is used to calibrate the test. Namely, it is used to specify the signal region \mathbb{S} in eq. (3) and the degree K of the basis, see eq. (99). The signal region is fixed to be the interval between the 10% and 90% quantiles of the empirical signal distribution in the validation dataset. That is, we allow for 20% of signal contamination in the control region. Inspecting the empirical distribution of the background, we find that the ratio between contamination and background in the control region, $\epsilon/B(\mathbb{C})$ in eq. (7), ranges between 0.21-0.23 for the high-mass resonance experiments and 0.29-0.3 for the decaying high-pT W-boson experiments. Thus, on average, we expect to underestimate the true signal strength by roughly 25%.

To fix the degree of the basis, we sub-sample N datasets of n background observations from the validation dataset. That is, these datasets follow the null distribution. Given $X_1, \dots, X_n \sim f$, let $\Psi_\alpha^{(K)}$ denote a test defined by eq. (9), where the parametric background (eq. (55)) is given by the Bernstein polynomial basis (eq. (99)). Then for $K \in \{5, 10, 15, 20, 25, 30, 35, 40\}$, we compute the empirical type-I error probability and choose K such that the corresponding test is closest to the desired type-I error rate. Con-

cretely, we use the test $\Psi_\alpha^{(K*)}$, where

$$K_* = \arg \min_K \left| \alpha - \frac{1}{N} \sum_{j=1}^N \Psi_\alpha^{(K)} (F_n^{(j)}) \right| \quad (100)$$

and $F_n^{(j)}$ is the empirical distribution of $\left\{X_i^{(j)}\right\}_{i=1}^n$. For all forthcoming experiments, we set $\alpha = 0.05$, $n = 20000$ and $N = 500$. Given the above test, a signal-enriched test can be built by first filtering observations using the trained classifier and then applying the test. Namely, $\Psi_\alpha^{(K*)}(X, t) = \Psi_\alpha^{(K*)}(\tilde{X})$ where $X_i \in \tilde{X}$ if $I(T_M(h(X)) \geq q(t))$. Thus, conditioned on the training and validation dataset, $\Psi_\alpha^{(K*)}(\cdot, t)$ is a deterministic function. Note that the signal-enriched test maintains approximate validity due to the decorrelation algorithm preserving the shape of the background distribution.

Using the test dataset, we study the power of the signal-enriched test and the performance of the CDOT decorrelation algorithm. To analyze the power of the signal detection test, we proceed as follows: given a signal strength λ , we sub-sample N datasets of n observations from the test dataset, such that $\lambda\%$ of those observations correspond to signal events. Then, for each dataset, we check if the test rejects the null hypothesis $H_0 : \lambda = 0$ and compute the empirical probability of rejecting the null hypothesis across datasets. Note that for $\lambda = 0$, that probability is the empirical type-I error, while for $\lambda \in \{0.01, 0.02, 0.05\}$ is the empirical power. In all cases, we report the empirical results with their corresponding Clopper–Pearson confidence intervals. Finally, to understand the utility of the decorrelation algorithm, we study the power of the signal-enriched test both when using a non-decorrelated and decorrelated classifier to filter the observations.

D.4 W-tagging dataset

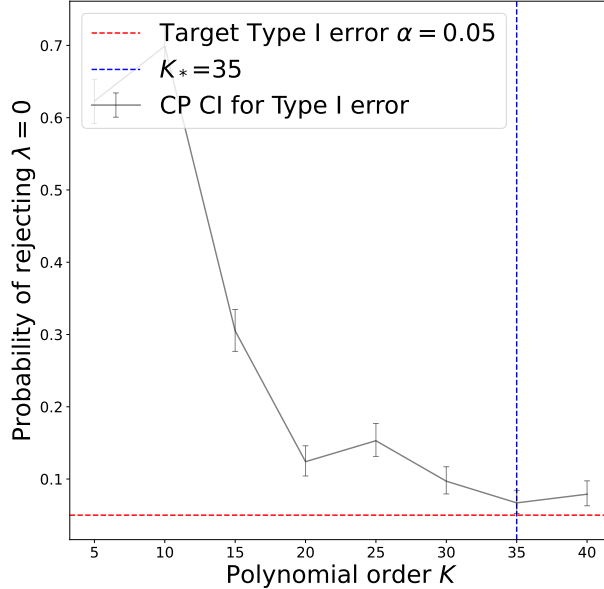


Figure 14: Model selection using simulated datasets composed only of background observations from the W-tagging validation dataset. The target type-I error rate is 0.05. However, none of the asymptotic tests achieve it. The Bernstein basis of order 35 is selected, which achieves an average type-I error rate between 0.05 and 0.1.

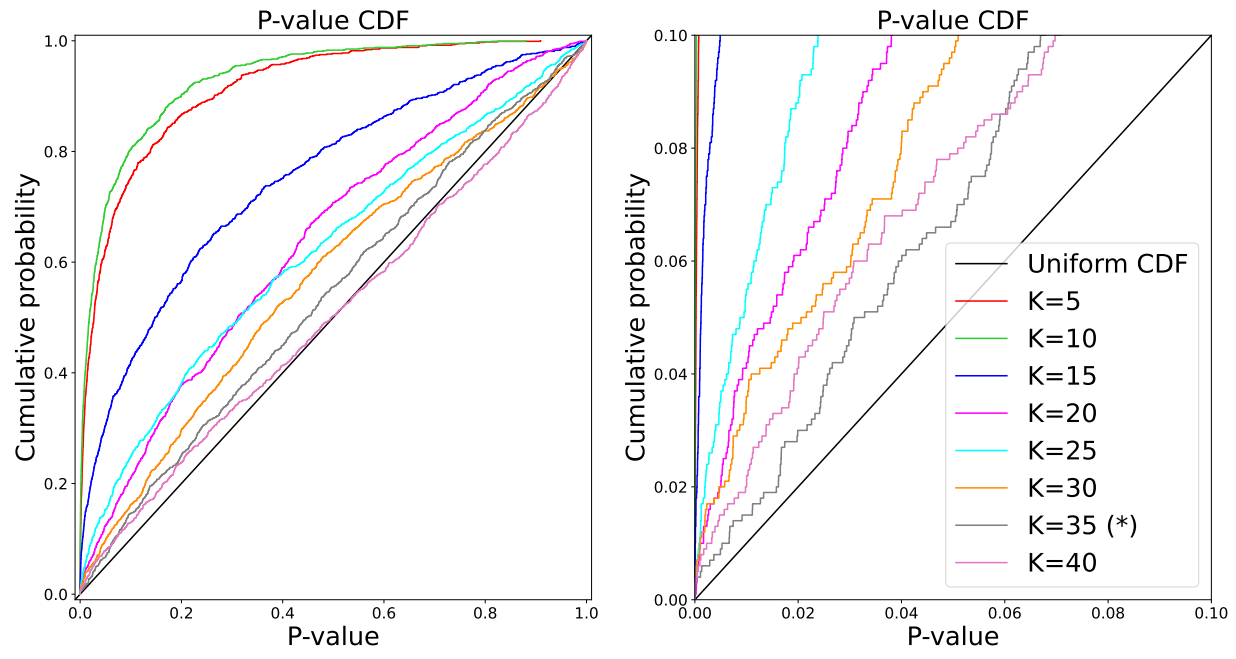


Figure 15: CDFs of the empirical p-value distributions corresponding to the different tests considered in Figure 14.

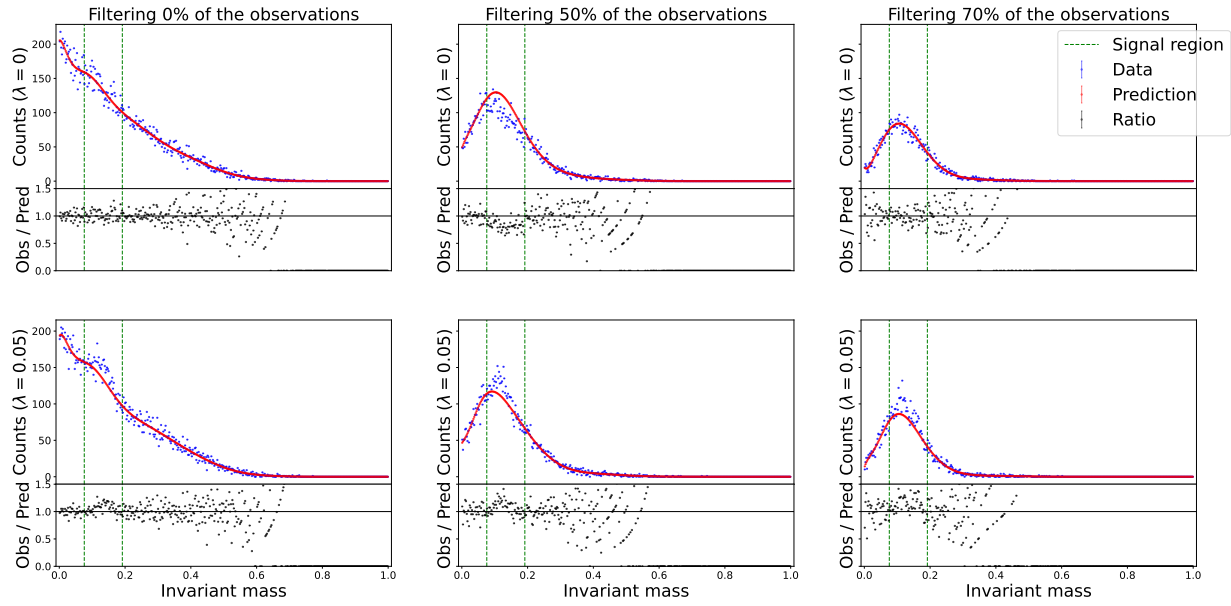


Figure 16: Single background estimate for the W-tagging test dataset as the number of observations filtered by the **non-decorrelated** classifier is increased. The first row corresponds to the null hypothesis, i.e., no signal. In the second row, 5% of the data comes from the signal. Note that the shape of the background distribution does not change.

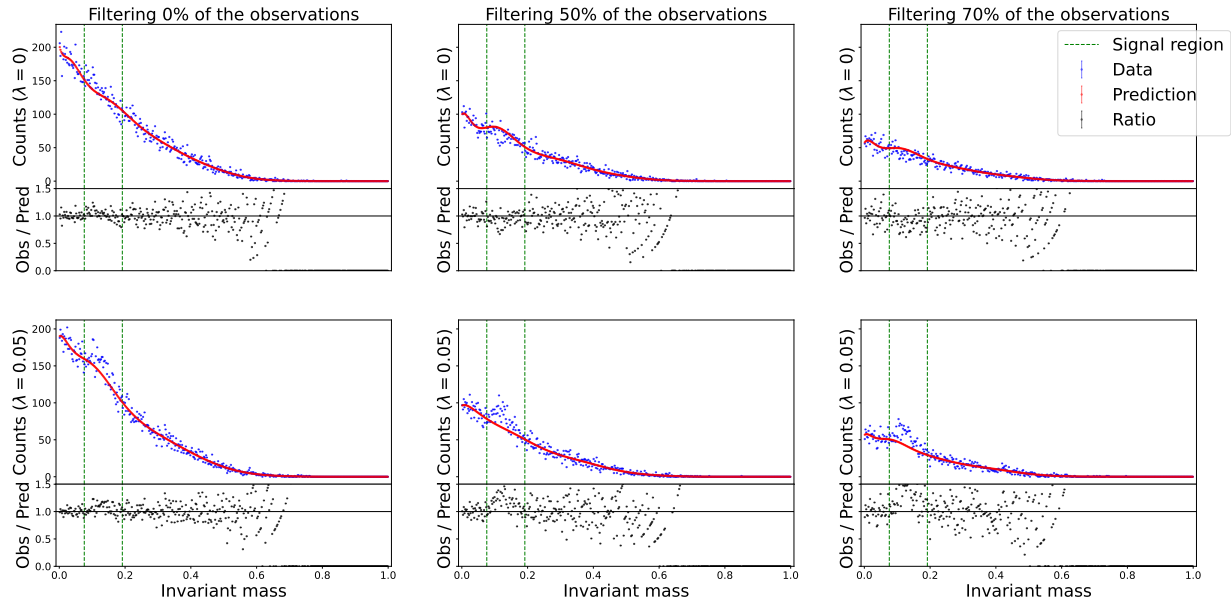


Figure 17: Single background estimate for the W-tagging test dataset as the number of observations filtered by the **decorrelated** classifier is increased. The first row corresponds to the null hypothesis, i.e., no signal. In the second row, 5% of the data comes from the signal. Note that the shape of the background distribution does not change.

D.5 3b and 4b datasets

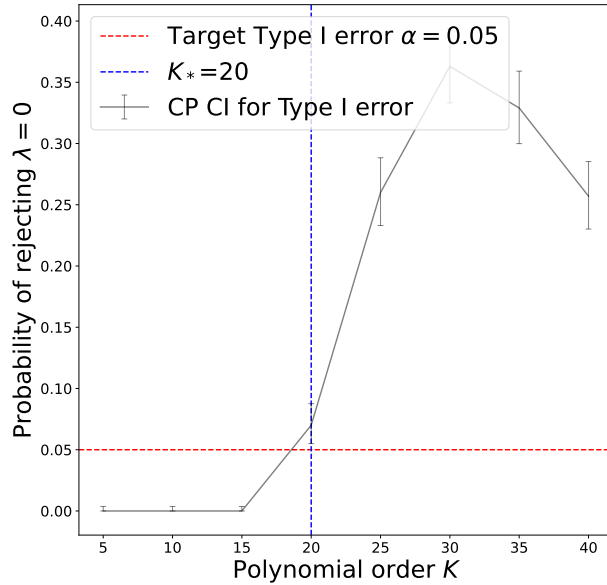


Figure 18: Model selection using simulated datasets composed only of background observations from the 3b validation dataset. The target type I error is 0.05. Bernstein basis of order 20 is selected.

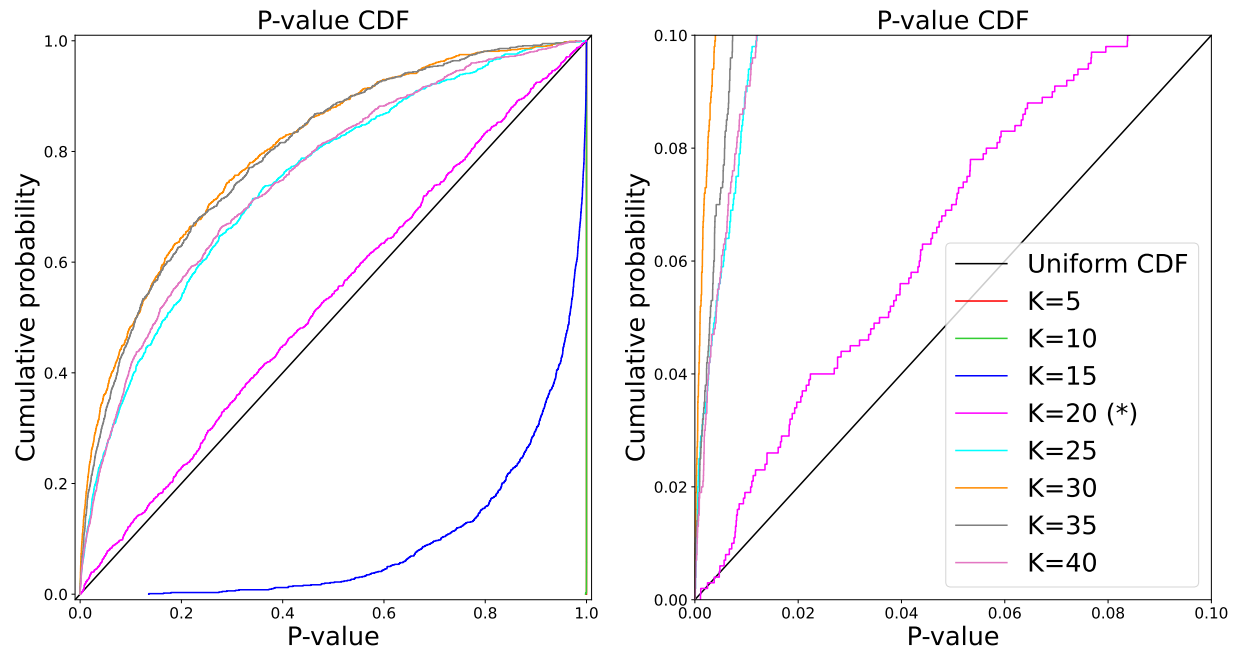


Figure 19: CDFs of the empirical p-value distributions corresponding to the different tests considered in Figure 18.

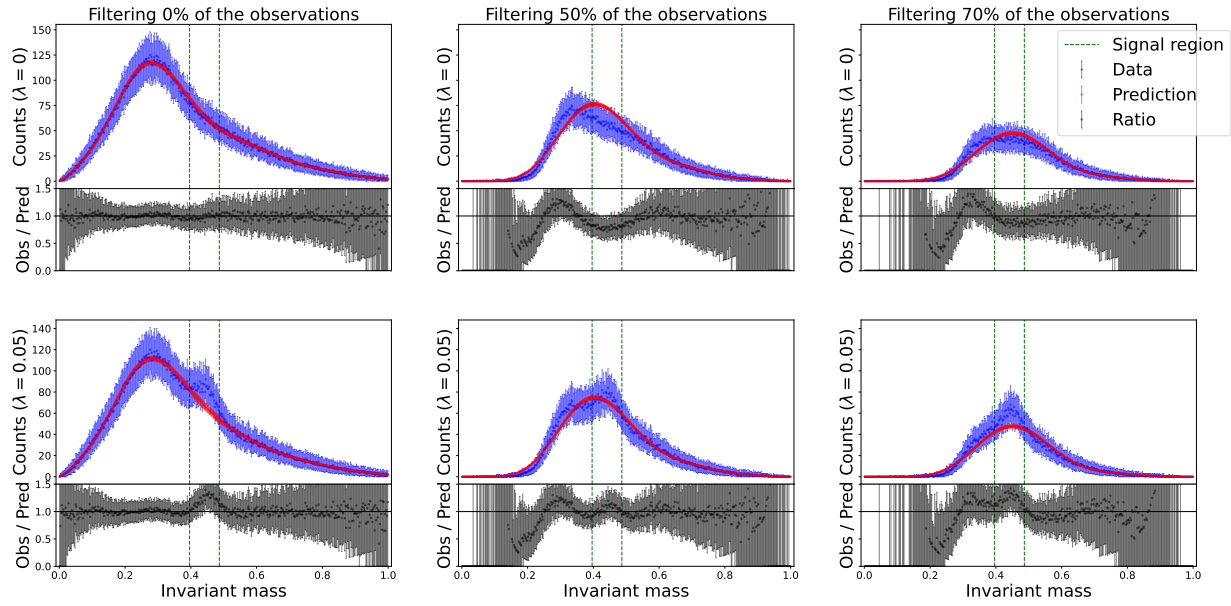


Figure 20: Background estimates for the 3b test dataset as the number of observations filtered by the **non-decorrelated** classifier is increased. The first row corresponds to the null hypothesis, i.e., no signal is present. In the second row, 5% of the data comes from the signal distribution. Note that the shape of the background distribution changes, producing a bump in the signal region. The intervals are 95% variability intervals based on 1000 simulations, and their midpoint is the median of the simulations.

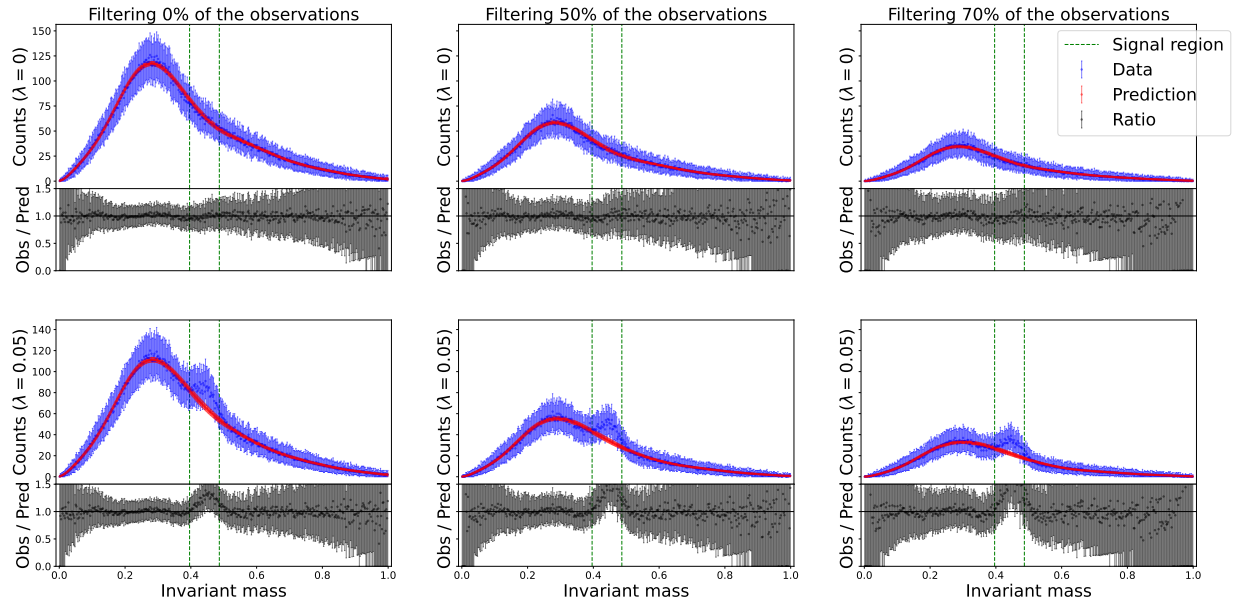


Figure 21: Background estimates for the 3b test dataset as the number of observations filtered by the **decorrelated** classifier is increased. The first row corresponds to the null hypothesis, i.e., no signal. In the second row, 5% of the data comes from the signal. Note that the shape of the background distribution does not change. The intervals are 95% variability intervals based on 1000 simulations, and their midpoint is the median of the simulations.

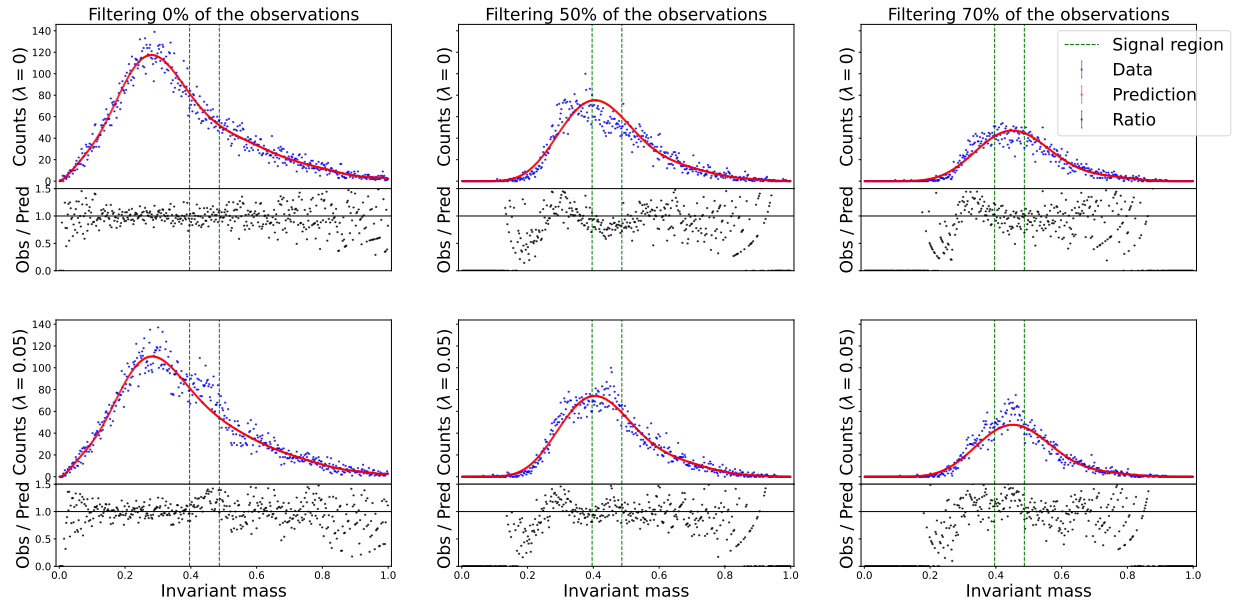


Figure 22: Single background estimate for the 3b test dataset as the number of observations filtered by the **non-decorrelated** classifier is increased. The first row corresponds to the null hypothesis, i.e., no signal. In the second row, 5% of the data comes from the signal. Note that the shape of the background distribution does not change.

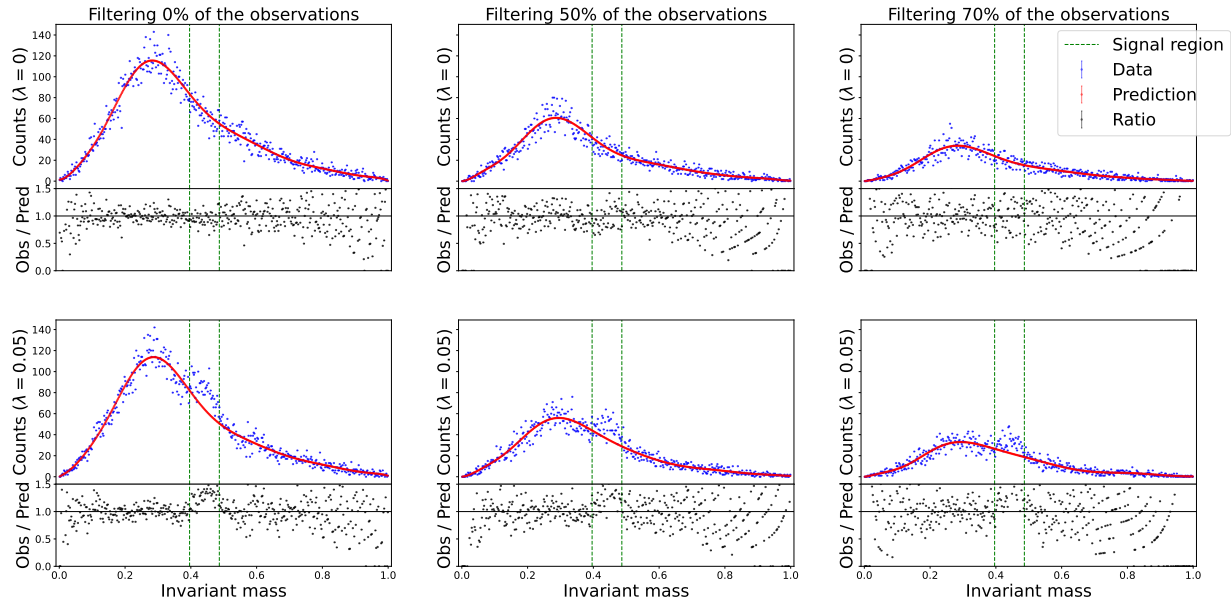


Figure 23: Single background estimate for the 3b test dataset as the number of observations filtered by the **decorrelated** classifier is increased. The first row corresponds to the null hypothesis, i.e., no signal. In the second row, 5% of the data comes from the signal. Note that the shape of the background distribution does not change.

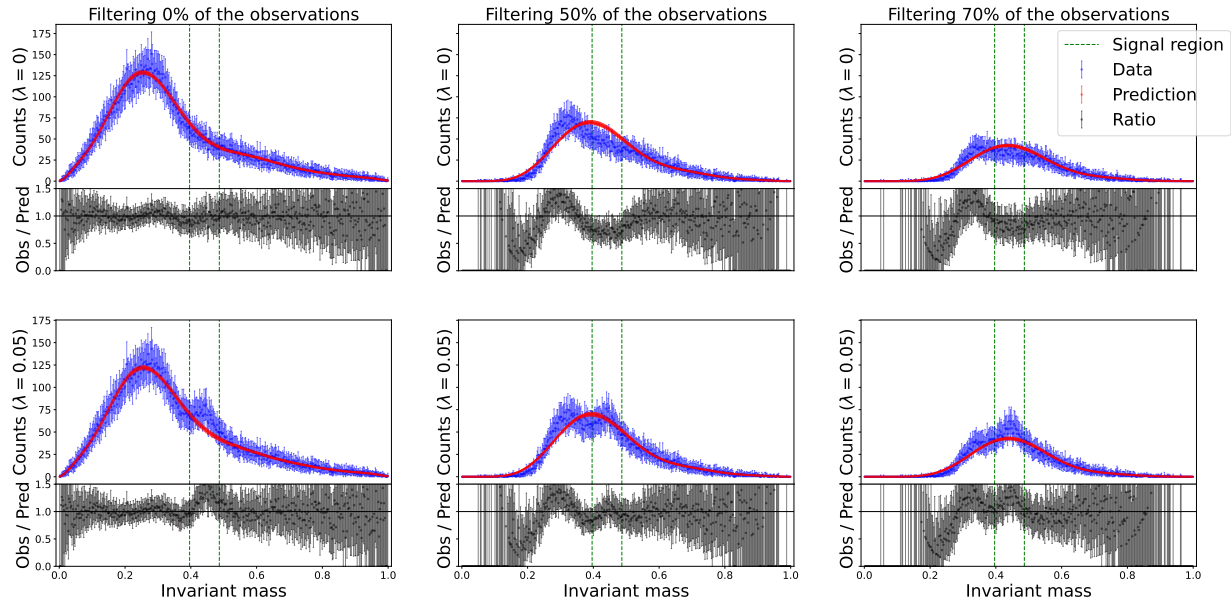


Figure 24: Background estimates for the 4b test dataset as the number of observations filtered by the **non-decorrelated** classifier is increased. The first row corresponds to the null hypothesis, i.e., no signal is present. In the second row, 5% of the data comes from the signal distribution. Note that the shape of the background distribution changes, producing a bump in the signal region. The intervals are 95% variability intervals based on 1000 simulations, and their midpoint is the median of the simulations.

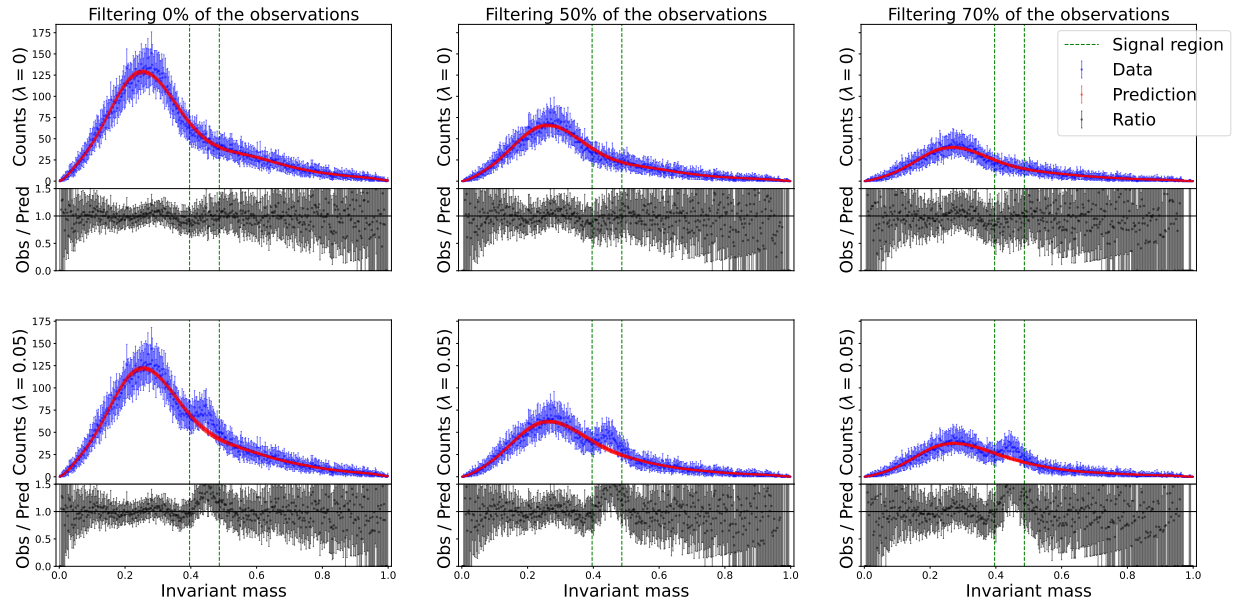


Figure 25: Background estimates for the 4b test dataset as the number of observations filtered by the **decorrelated** classifier is increased. The first row corresponds to the null hypothesis, i.e., no signal. In the second row, 5% of the data comes from the signal. Note that the shape of the background distribution does not change. The intervals are 95% variability intervals based on 1000 simulations, and their midpoint is the median of the simulations.

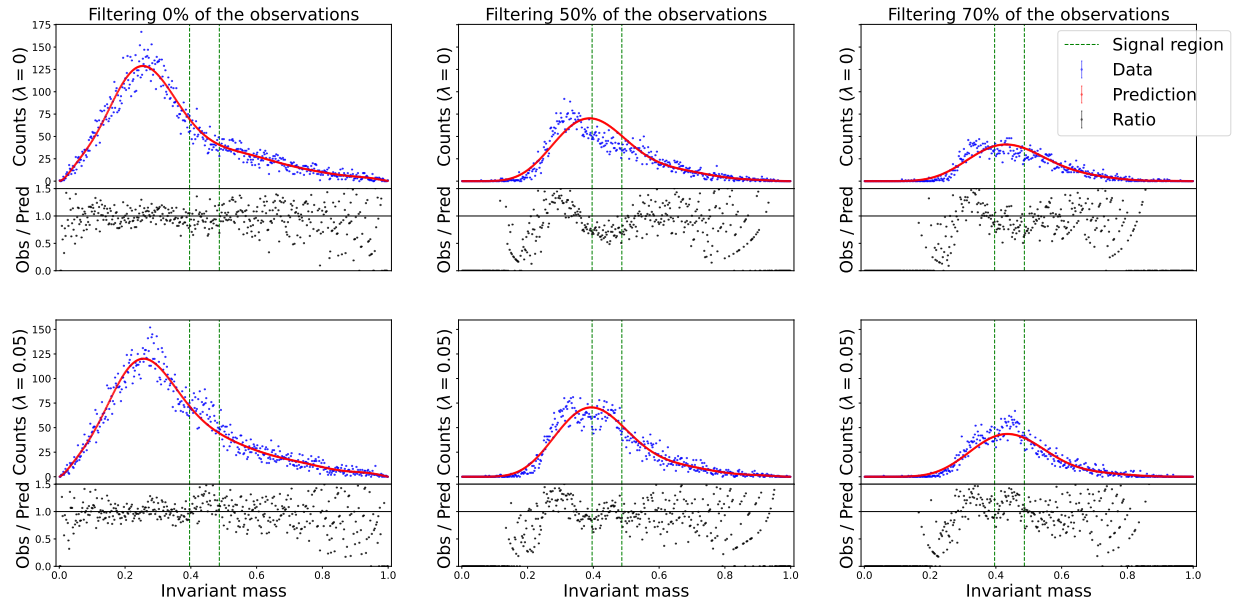


Figure 26: Single background estimate for the 4b test dataset as the number of observations filtered by the **non-decorrelated** classifier is increased. The first row corresponds to the null hypothesis, i.e., no signal. In the second row, 5% of the data comes from the signal. Note that the shape of the background distribution does not change.

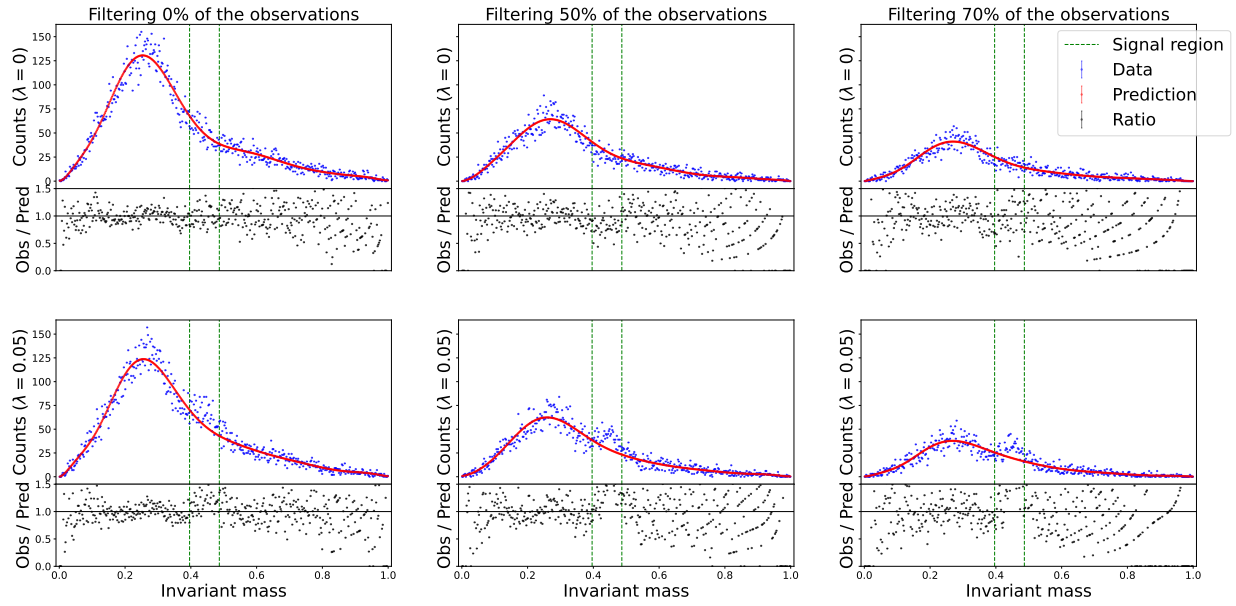


Figure 27: Single background estimate for the 4b test dataset as the number of observations filtered by the **decorrelated** classifier is increased. The first row corresponds to the null hypothesis, i.e., no signal. In the second row, 5% of the data comes from the signal. Note that the shape of the background distribution does not change.